Interfacial behaviours of ionic fluids

Theory and simulations

Stenberg, Samuel

2022

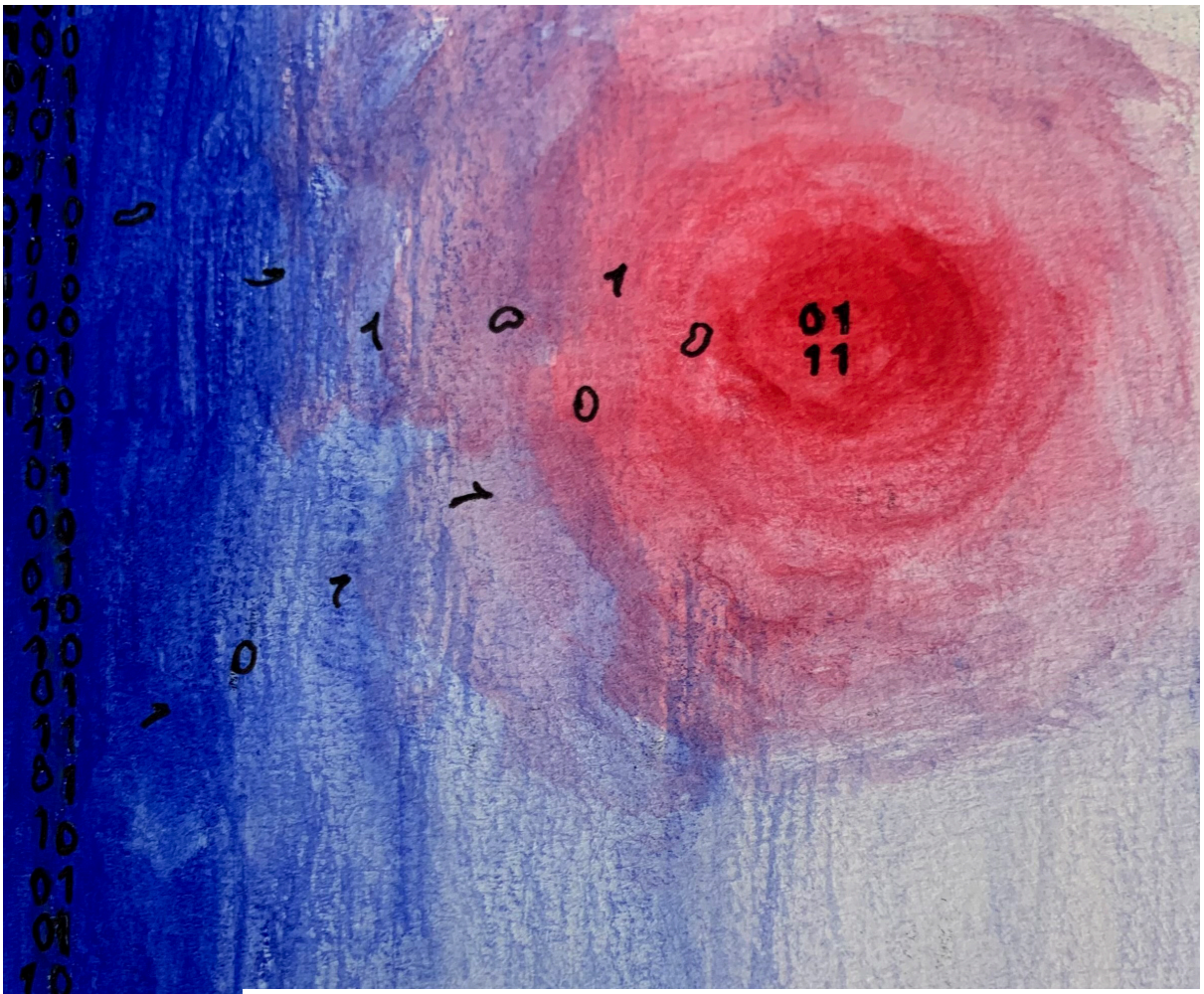

Interfacial behaviours of ionic fluids

Theory and simulations

SAMUEL STENBERG | DIVISION OF THEORETICAL CHEMISTRY | LUND UNIVERSITY

Interfacial behaviours of ionic fluids

Interfacial behaviours of ionic fluids
Theory and simulations

by Samuel Stenberg

LUND
UNIVERSITY

Doctoral Thesis

by due permission of the Faculty of Science of Lund University. To be defended for public criticism in lecture hall A, Kemicentrum on wednesday, the 25th of May 2022 at 09:15.

Faculty opponent
Prof. Mathieu Salanne
Sorbonne Université, France

DOKUMENTDATABLAD enl SIS 61 41 21

Organization
LUND UNIVERSITY
Department of Chemistry
Box 124
SE–221 00 LUND
Sweden

Author(s)
Samuel Stenberg

Document name
DOCTORAL THESIS

Date of disputation
2022-05-25

Sponsoring organization

Title and subtitle
Interfacial behaviours of ionic fluids Theory and simulations

Abstract
This thesis and the papers included is an *in silico* study of how charged particles interact and behave close to surfaces, and how to treat these interactions in simulations. This type of systems is found in widely different contexts, from capacitors to biological cells. The knowledge about such systems is therefore very important, as it affects many different areas, not in the least in science. In this thesis, new methods on how to include interactions between charged particles and conducting surfaces in simulations are presented. These methods are then used to study how ions interact and behave when confined by surfaces.

Key words
statistical thermodynamics, molecular simulation, Markov chains, Monte Carlo simulations, electrostatics, Ewald summation, ionic fluids, ion correlations

Classification system and/or index terms (if any)

Supplementary bibliographical information

Language
English

ISSN and key title

ISBN
978-91-7422-888-5 (print)

Recipient's notes

Number of pages
140

Price

Security classification

Signature Samuel Stenberg

Date 2022-04-11

Interfacial behaviours of ionic fluids

Theory and simulations

by Samuel Stenberg

LUND
UNIVERSITY

A doctoral thesis at a university in Sweden takes either the form of a single, cohesive research study (monograph) or a summary of research papers (compilation thesis), which the doctoral student has written alone or together with one or several other author(s).

In the latter case the thesis consists of two parts. An introductory text puts the research work into context and summarizes the main points of the papers. Then, the research publications themselves are reproduced, together with a description of the individual contributions of the authors. The research papers may either have been already published or are manuscripts at various stages (in press, submitted, or in draft).

Cover illustration front: "Binary Attraction" by Josefin Ahnlund.

Cover illustration back: "Binary Potential" by Josefin Ahnlund.

Parts of this thesis has been published before in: Stenberg, Samuel, *Electrostatic Interactions; and ways to account for them (2020)*.

Funding information: The thesis work was financially supported by the Swedish Research Council.

Faculty of Science, Department of Chemistry

ISBN: 978-91-7422-888-5 (print)

Printed in Sweden by Media-Tryck, Lund University, Lund 2022

Media-Tryck is a Nordic Swan Ecolabel certified provider of printed material. Read more about our environmental work at www.mediatryck.lu.se

Printed matter 3041 0903

MADE IN SWEDEN

Till Josefin
För att det inte vore möjligt utan dig

Contents

List of publications

This thesis is based on the following publications, referred to by their Roman numerals:

I **An Exact Ewald Summation Method in Theory and Practice**

S. Stenberg, B. Stenqvist
The Journal of Physical Chemistry A, 2020, 124(19), pp. 3943-3946

II **Grand canonical simulations of ions between charged conducting surfaces using exact 3D Ewald summations**
S. Stenberg, B. Stenqvist, C. E Woodward and J. Forsman
Physical Chemistry Chemical Physics, 2020, 22(24), pp. 13659-13665

III **Overcharging and Free Energy Barriers for Equally Charged Surfaces Immersed in Salt Solutions**
S. Stenberg and J. Forsman
Langmuir, 2021, 37, pp. 14360-14368

IV **Interactions between conducting surfaces in salt solutions**

S. Stenberg, C. E Woodward and J. Forsman
Soft Matter, 2022, 18, pp. 1636-1643

V **Simulations of phase transitions and capacitance, of simple ionic fluids in porous electrodes.**
S. Stenberg, P. Vo, C. E Woodward and J. Forsman
Manuscript

Populärvetenskaplig sammanfattning på svenska

Nästan allt du kan tänka dig är uppbyggt utav atomer. Tillsammans bygger dessa atomer olika ämnen och material, inte helt olikt legobitar. Om vi vill förstå den värld vi lever i, är det därför viktigt att vi förstår hur dessa atomer beter sig i olika omgivningar.

Det finns olika typer av forskning för att studera atomers och molekylers beteenden. Den mest kända är kanske genom experiment i ett laboratorium. Ofta kan det dock vara svårt att på en atomistisk nivå se exakt vad som händer när man till exempel blandar två kemikalier. Detta för att atomer är både väldigt små och rör sig otroligt snabbt. Det är också svårt att kontrollera vissa parametrar i ett verkligt experiment, till exempel antalet atomer, eller en exakt temperatur. Det är av dessa anledningar som vi gör datorsimuleringar. I en datorsimulering kan vi, på en atomistisk nivå, se exakt hur atomer beteer sig under de exakta betingelser vi är intresserade utav. Så hur gör man då en datorsimulering av så små partiklar? Först måste vi veta vad som får dem att röra på sig, dvs, hur de interagerar.

Precis som planeter (som ju faktiskt består av atomer) så interagerar atomer och molekyler med varandra. Det är dessa interaktioner som bestämmer hur en atom rör sig, precis som att det är interaktionen mellan jorden och solen som bestämmer hur jorden rör sig. Det finns olika typer av interaktioner, men den starkaste interaktionen (i ett klassiskt ramverk) kallas för elektrostatisk interaktion. Det är också denna typ av interaktion som i huvudsak diskuteras i denna avhandling. Elektrostatisk interaktion finns mellan två elektriskt laddade partiklar. Denna interaktion är långväga. Ordet långväga betyder i denna kontext att den har en stor utbredning i rummet, dvs två partiklar långt ifrån varandra kommer i huvudsak att interagera via elektrostatiska krafter.

Så om vi nu vet hur partiklar interagerar med varandra, då är det bara att köra på, eller? I ett glas vatten finns det ungefär 10^{24} vattenmolekyler (en etta med 24 nollor efteråt!), det är ungefär lika många stjärnor som finns i universum. Att simulera ett så tillsynes enkelt fall som ett glas vatten skulle därför ta otroligt lång tid (många år, även för den snabbaste datorn i världen). Den största boven i dramat är just interaktionen mellan atomer. För att simulera det tidigare nämnda glas vatten behöver vi räkna ut interaktionen mellan alla atomer. Det betyder att vi måste räkna ut $\binom{10^{24}}{2} = \frac{10^{24}!}{(10^{24}-2)!2!} \approx 5 * 10^{47}$ interaktioner, en enorm siffra! När vi gör datorsimuleringar måste vi därför göra antaganden som förenklar de kemiska system vi är intresserade utav. Den första delen av denna avhandling syftar till att hitta nya sätt att ta hänsyn till elektrostatiska interaktioner under olika betingelser. I den andra delen kommer vi att fokusera på en speciell kategori av kemiska system; nämligen hur laddade partiklar beter sig nära ytor. Denna typ av system finns överallt, i allt ifrån kondensatorer i elektriska kretsar, till cellerna i våra kroppar. Speciellt så kommer vi

i denna del att använda de nya metoder vi utvecklat för att studera dessa typer av system.

Interfacial behaviours of ionic fluids Theory and simulations

Chapter 1

Introduction

Theoretical Chemistry may seem as a counterintuitive term, as Chemistry has a strong archetype of a person in a white lab coat mixing chemicals together. At least that was my belief when i started to study chemistry. So what is theoretical chemistry, and why does it exist?

In an experimental setup it can be hard to control certain parameters, for instance temperature, pressure or the number of particles, or to get insight at a molecular level. However, in a simulation setup we have complete control over all parameters and a very detailed view of what is happening at the molecular/atomic level. Sometimes we can even predict the result of an experiment. The only thing we have to worry about is that our model is good enough to realistically reproduce the property or behaviour that we wish to investigate. This is actually a very complex problem and as of now, there is no "complete unified model", but there are many different models which are good at different things and (sometimes very) bad at others. A good example of this is the simulation of water, of which there exist many different models. Some water models are able to accurately reproduce some property A, but fail to reproduce another property B. Then of course there are models which reproduce property B but fail to predict A [1,2,3,4]. Nevertheless, not to discourage the reader too much, molecular simulation is an increasingly important field of science, and has helped us, and continues to help us, understand and predict important outcomes in chemistry, physics and biology.

So how do we run a simulation? First of all we need to define a simulation box (or sphere or any other geometry, I write box here because cubic simulation boxes are common), containing the particles we wish to simulate. If we were to not confine the particles in our simulation, they would simply spread out indefinitely. This would

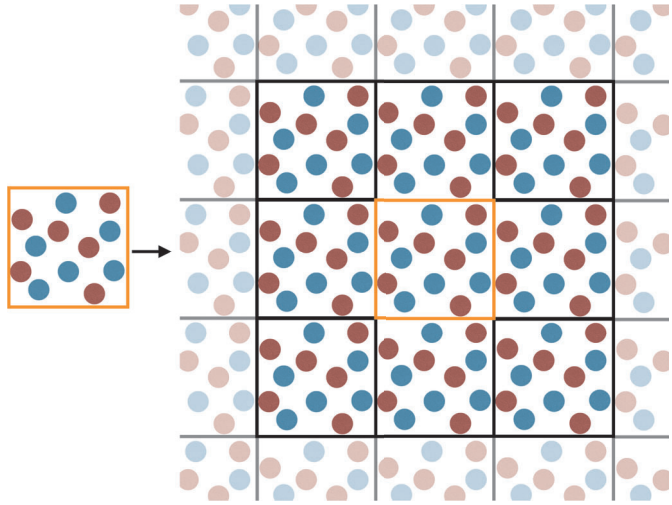

Figure 1.1: Illustration of 2-dimensional periodic boundary conditions (PBC). The leftmost orange box represents the simulation box and the blue and red circles represent particles. In the right figure the simulation box is replicated in space.

correspond to infinite dilution and we would never be able to accurately compute properties in such a system. Further, in real experiments the number of particles is huge, on the order 10^{23}, this is way too much for a computer to handle. Hence we need to limit the size of our system while still trying capture the main characteristics. A side effect of this confinement is that we get unwanted boundaries or "walls" in our simulation. We can remove the boundaries by using periodic boundary conditions (PBC). When using PBC, a particle that travels outside a boundary gets reflected back into the box on the opposite side. This way, there are no "physical" boundaries in our simulation. Still we have the problem that our system is much smaller than a real system. This effectively means that there are no long range interactions, which in turn affects the behaviour of the particles and gives rise to size effects. Size effects can be mitigated by extending interactions to an infinite system in which the simulation box is replicated in space. This procedure forms (in theory) an infinite lattice with our simulation box as the unit cell, see fig. 1.1. Calculating the energy between the particles in such a system results in an infinite sum (because there are an infinite number of particles), and one has to, in practice, use a cutoff value. A fairly common approach to implement such a cutoff, is to use the minimum image convention, where each particle interacts with the nearest copies of the surrounding particles.

This thesis will focus on how charged particles (ions) interact and behave in a system where hard surfaces are present. The charged particles encountered here are rough models of real ions.

To better understand the approximations involved, and the theory behind simulations

we will in the next few chapter present the basis of molecular simulation in more detail. The next chapter will present basic theory of thermodynamics, which lays the foundation for relations that we use to calculate the properties that we are interested in. We will also look into one of the two main driving forces that we are interested in, entropy. In Chapter 3, the second driving force is presented, energy, and how we can reduce size effects. Chapter 4 presents the details on how to perform a simulation, and the theory behind it, with a focus on Markov Chain Monte Carlo simulations. In Chapter 5 we will look into a different way to calculate molecular properties, called classical Density Functional Theory. In Chapter 6 we get a bit more practical and present the actual molecular systems of interest, and why they are important.

Chapter 2

Thermodynamics

Even considering the approximations mentioned in the last section, molecular simulation is a time demanding task. Often we are interested in an average of some property A which is a function of the coordinates and momenta of all particles $\Gamma = \left(\mathbf{r}^N,\ \mathbf{p}^N\right)$, where N is the number of particles. The collection of variables Γ is often referred to as a *microstate*. Each microstate is a point in a multidimensional *phase space* $\mathcal{S}$, in which the dimensions represent all the components of the coordinates and momenta of all particles. Hence, for a 3-dimensional system, phase space contains $6N$ dimensions. Using these definitions we can construct an average, of a mechanical variable, as a function of the microstates

$$\langle A(\Gamma)\rangle = \int_{\mathcal{S}} A(\Gamma)P(\Gamma)d\Gamma, \tag{2.1}$$

where $P(\Gamma)$ is some appropriate probability distribution describing the probability of observing the microstate Γ. In most practical cases the integration in eq. 2.1 has to be performed in many hundreds, thousands or even more dimensions, since Γ has $6N$ degrees of freedom. Therefore analytical solutions to eq. 2.1 is not feasible, but has to be approximated. In practice this amounts to sampling A from the system of interest using the probability distribution $P(\Gamma)$. As it turns out, in many cases it is enough to sample around the points where $P(\Gamma)$ is the largest, since $\langle A(\Gamma)\rangle$ will be dominated by the values at these points. To achieve this, we will in this thesis focus on a method called *Metropolis Monte-Carlo*, which is presented in Chapter 4. In this chapter and the next, we will present, what we in this thesis will refer to as "the two main thermodynamic properties" which are important when determining $P(\Gamma)$, the energy and the entropy. How these two properties relate to the observables we are interested in is derived in the theory of thermodynamics.

The foundation of molecular simulation is thermodynamics. It is from thermodynam-

ics that equations describing properties of the systems that we simulate, are derived. Thermodynamics was first developed to describe the efficiency of steam engines. This included the relation between work, heat and energy. It also defines the important property of *entropy*, which will be introduced in the next section. Thermodynamics is now used in almost all fields of science, and allows descriptions and predictions of many different reactions and systems.

Before diving too deep into thermodynamics, we take a step back and look at the physical properties that we use to describe our systems. Since thermodynamics (and many other areas of science) is centered around describing different systems of different sizes and compositions, it is important that we can compare these systems and their properties. To compare systems of different size, or describe processes, it is convenient to have properties that scale with system size, and properties that do not, i.e that are only dependent on composition. This is the reason that we in mechanics and thermodynamics (and actually the majority of the physical sciences) mainly deal with two types of properties, extensive and intensive. Intensive properties do not scale with system size, but only depend on composition. Extensive properties, however, scale with the system size, such that $A(\lambda\mathcal{P}) = \lambda A(\mathcal{P})$. Here λ is a scaling parameter, and $\mathcal{P}$ is the collection of all properties that determines the size of the system (hence all properties $\mathcal{P}$ are also extensive). As we shall see later, the intensive properties are not unlike forces, while the extensive properties are coordinates, able to react to those forces. It is, though, important to remember that not all properties are intensive or extensive. Most of the observables discussed in this thesis can be categorized as either intensive or extensive. For a more thorough discussion about extensive and intensive properties, see the paper by Redlich[5], and references therein.

In the next section we introduce the first main thermodynamic property, entropy. This will be our starting point for thermodynamics.

2.1 Entropy

Entropy is an eluding concept, even though we use it to describe one of the most fundamental properties in the universe. At its heart, entropy is something tangible and we can observe its effects with a simple example.

Consider a collection of two types of particles, A and B, occupying a room. The two different types of particles can be distinguished from one another by some observable property. The particles do not interact with each other, and also does not occupy any volume (they are so-called *ideal*). The room has a constant size and is closed so that no particles can leave or enter the room. The particles collide elastically with the boundaries of the room, and there is no energy transfer in such collisions. Hence the number of particles, volume of the room and total internal energy (i.e the sum of

the kinetic energies of all particles) are constant. Since the particles do not interact with each other, there are no correlations and their movement can be considered as random. This in turn means that all microstates are equally likely, since there is no preference for any single microstate or subset of microstates.

Now imagine partitioning phase space into two subspaces. The first subspace contains all microstates where all molecules A occupy the left half of the room, and all molecules B occupy the right. In the second subspace all particles are equally mixed. The second subspace obviously contains more microstates than the first. Hence the second subspace has a higher probability of being observed, since all microstates have the same probability of being occupied. This turns out to be true for all system where N, V and U are constant, even if the particles are not ideal, see note. 2.1. The collection of all available microstates in a system where N, V and U are constant is called a *microcanonical ensemble*.

Note 2.1. Equal a priori probabilities

It is a basic assumption in thermodynamics that all microstates in the microcanonical ensemble have the same probability of being observed. We can motivate this with an example (albeit a very theoretical one).
Consider a Molecular Dynamics[6] (MD) simulation (with not necessarily ideal particles) with an infinitely small time step, performed on a computer that has infinite precision. The simulation is propagated with Newtons equations of motion, which are deterministic and preserves energy. As the system is propagated all accessible microstates will be visited "in order" to finally end up in the starting state again. Each cycle every microstate is visited exactly once. If it did not, the system would not be in equilibrium. The same cycle through the microstates will be repeated until the simulation is stopped, due to the deterministic nature of MD. This means that all microstates will be visited equally often, and thus have the same probability of begin observed.
From a theoretical point of view, this would mean that, in all simulations which are exactly deterministic, the probability of observing a microstate is the same for all microstates. In practice, however, it is not possible to perform a simulation which is exactly deterministic due to the finite precision of computers.

This can be illustrated by plotting the number of microstates against the fraction of A molecules in the right side of the box, χ, which is shown in fig. 2.1. From this figure it is clear that the number of states increases as the particles become more equally distributed, and reaches a maximum at $\chi = 0.5$, where each side consists of 50% A molecules and 50% B molecules. Hence we say that the system has a driving force which (on average) drives the system towards a more mixed state. This driving force is

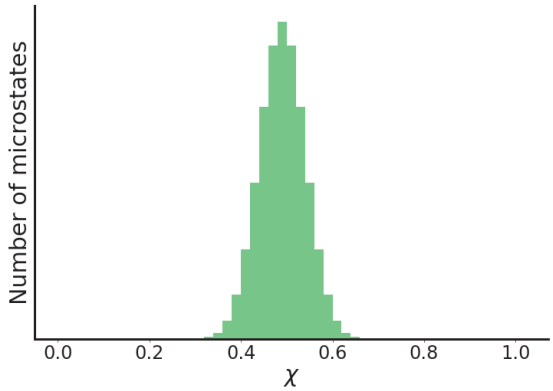

Figure 2.1: Number of states plotted against the fraction of particles in the second subspace.

due to a difference in *entropy* of the two subspaces and points in the direction towards maximum entropy. When the entropy is at maximum, the system has maximized its available number of microstates, hence in a way, maximized its freedom. Note that the entropy of the combined system in this example is constant. This entropy will however be dominated by the mixed state.

It is also useful to quantify the entropy. Lets denote the total number of accessible microstates as Ω, the probability is then $1/\Omega$. The entropy is then *defined* as the logarithm of the total number of accessible microstates (which is proportional to the phase space volume).

$$S = k_B \ln(\Omega) \tag{2.2}$$

where k_B is the Boltzmann constant. The entropy measure above is usually called the *Boltzmann entropy*.

Eq. 2.2, however, presents a problem. From a classical point of view, space (and energy) is continuous, and hence there is an infinite number of possible configurations. This would be true regardless of system size, as long as the size of the system is larger than zero in any dimension. This means that the entropy would be infinite for practically any system, which would render the entropy a pretty useless concept. Due to this reason, phase space has historically been discretized, which in turn rendered the entropy finite. This discretization can now be motivated by quantum mechanics and the Heisenberg uncertainty principle, which states that there is a finite precision to which we can determine position and momenta simultaneously:

$$\Delta p \Delta x \sim h.$$

where h is Planck's constant. This means that the smallest area that one can define

in phase space is h (or a (hyper)volume h^3 in the case of a particle which has three degrees of freedom)[7]. Hence when integrating over the phase space, the final value is divided by h^D, where D is the dimensionality.

To get a more detailed view on entropy, lets take a more concrete example. Consider a volume V, divided into $\mathcal{L}$ available lattice points, and N particles of the same type. The particles are allowed to occupy the same lattice point, and they do not interact. The number of microstates, Ω, of such a system is

$$\Omega = \mathcal{L}^N$$

since each particle can be placed in $\mathcal{L}$ different locations.

From a purely observational point of view, entropy is an extensive quantity, hence if one double the system size one also doubles the entropy. This is trivially true for non interacting systems. Consider for instance doubling the example above. The total number of microstates is then Ω^2 which gives the total entropy $S_T = k \ln(\Omega^2) = 2S$. If we instead double the size of the system, according to eq. 2.2 one should have:

$$2 \ln\left(\mathcal{L}^N\right) \text{ equal to } \ln\left((2\mathcal{L})^{2N}\right)$$

This is obviously not true since $2 \ln\left(\mathcal{L}^N\right) = \ln\left(\mathcal{L}^{2N}\right)$. Hence we also gain entropy from the increased number of states due to the mixing (or rather the left hand side of the above equation only includes the perfectly mixed state of the larger system). This contribution is here 2^{2N}, or $2N \ln(2)$ to the entropy. This is known as Gibbs paradox.

To solve this, we include something called the indistinguishability of similar particles. When we double the system, the second system contains the same type particles as the first, and there is no way for us to tell them apart. If we have no way of determining any difference between two particles, swapping these two particles yields the same microtate.

To account for indistinguishable particles, we need to divide by the number of permutations, which is $N!$. This is however only true if the particles are not allowed to occupy the same state (position in this case). So what if we from the beginning tried to remove all the permutations which we cannot tell apart

$$2 \ln\left(\frac{(N+\mathcal{L}-1)!}{N!(\mathcal{L}-1)!}\right) \text{ equal to } \ln\left(\frac{(2N+2\mathcal{L}-1)!}{(2N)!(2\mathcal{L}-1)!}\right) \tag{2.3}$$

This is obviously not true either. So what is going on here? Well it turns out that the entropy is only extensive in the thermodynamic limit, i.e in the limit of infinite system size. In fig. 2.2 a similar plot as in fig. 2.1 is shown, but for different system

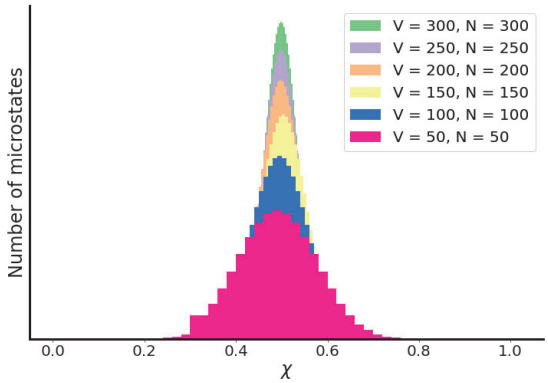

Figure 2.2: Histogram of the number of states calculated for different system sizes.

sizes. This figure illustrates that as the system size increases, the perfectly mixed state becomes more probable, i.e the standard deviation (or width) of the histograms decreases. Hence as the system size increases the total entropy is going to be increasingly dominated by the perfectly mixed state. This can be illustrated by plotting the ratio of the actual entropy and the entropy of the perfectly mixed state:

$$\Delta S(N, \mathcal{L}) = \frac{\ln\left(\frac{(2N+2\mathcal{L}-1)!}{(2N)!(2\mathcal{L}-1)!}\right)}{2\ln\left(\frac{(N+\mathcal{L}-1)!}{N!(\mathcal{L}-1)!}\right)}$$

in the thermodynamic limit, the perfectly mixed state is the only contributor to the entropy, as illustrated by fig. 2.3. In other words, if we double the size of the system, and only consider the perfectly mixed state of the larger system, the entropy is extensive.

A heavily used mathematical approximation in statistical thermodynamics is the Stirling approximation. It is used to approximate factorials, $x!$, and is in our case only relevant when x is an integer.

$$x! = \exp\left(x\ln\left(x\right) - x\right) \tag{2.4}$$

If we go back to eq. 2.3, but this time assume that $N >> 1$ and $\mathcal{L} >> 1$ such that $\mathcal{L} - 1 \approx \mathcal{L}$ and $N - 1 \approx N$, the equation instead reads:

$$2\ln\left(\frac{(N+\mathcal{L})!}{N!(\mathcal{L})!}\right) \text{ equal to } \ln\left(\frac{(2N+2\mathcal{L})!}{(2N)!(2\mathcal{L})!}\right)$$

Since we already assumed that N and $\mathcal{L}$ are very large, we can safely use the Stirling approximation, which renders the left and right hand side equal. Hence using the

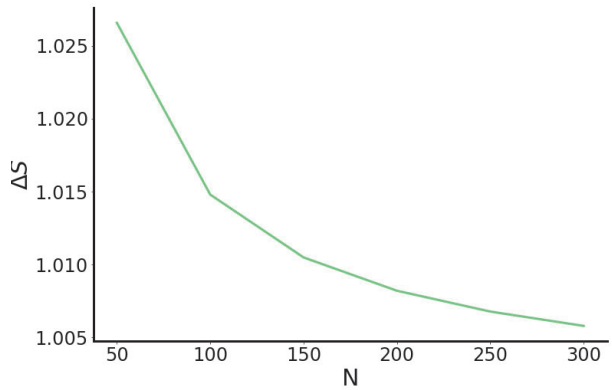

Figure 2.3: Histogram of the number of states calculated for different system sizes.

Stirling approximation is equivalent to neglecting the fluctuations from the perfectly mixed state. This is in many cases a fair assumption since at large $\mathcal{L}$ and N, the perfectly mixed state is dominating.

2.2 Equilibrium: The intensive variables

We now leave entropy and take a look at some other important properties. As stated in the beginning of this chapter, thermodynamics deals with systems in equilibrium. But what do we actually mean with equilibrium, and how do we determine if a system internally is in equilibrium, or that two systems are in equilibrium with each other? A simple way to define equilibrium would be to say that; in equilibrium there are no macroscopic flows of matter or energy from one part of the system to another. While on a microscopic level, instantaneous changes and flows occur all the time. To further investigate this, consider two systems which lie next to each other. The total entropy of the two systems is constant, but the individual entropies of the two systems can fluctuate. Consider also that the systems can exchange particles, while the total number of particles is held constant. The same goes for the volume, the total volume of the two systems is constant, but not that of the two systems separately. We can expand the differential of the total energy(for details, see the next section), dU, as the sum of the changes in energy of the two systems, dU_1 and dU_2

$$\begin{aligned} dU = dU_1 + dU_2 = \\ \left(\frac{\partial U_1}{\partial S_1}\right)_{V_1,N_1} dS_1 + \left(\frac{\partial U_1}{\partial V_1}\right)_{S_1,N_1} dV_1 + \left(\frac{\partial U_1}{\partial N_1}\right)_{S_1,V_1} dN_1 + \\ \left(\frac{\partial U_2}{\partial S_2}\right)_{V_2,N_2} dS_2 + \left(\frac{\partial U_2}{\partial V_2}\right)_{S_2,N_2} dV_2 + \left(\frac{\partial U_2}{\partial N_2}\right)_{S_2,V_2} dN_2 \end{aligned} \tag{2.5}$$

Since the total S, V and N are all constant, a change in one system has to be followed by an opposite change in the other system. Hence we have the following relations:

$$\begin{aligned} dS_1 &= -\, dS_2 \\ dV_1 &= -\, dV_2 \\ dN_1 &= -\, dN_2 \end{aligned}$$

Substituting the above relations into eq. 2.5 yields

$$dU = \left(\frac{\partial U_1}{\partial S_1} - \frac{\partial U_2}{\partial S_2}\right) dS_1 + \left(\frac{\partial U_1}{\partial V_1} - \frac{\partial U_2}{\partial V_2}\right) dV_1 + \left(\frac{\partial U_1}{\partial N_1} - \frac{\partial U_2}{\partial N_2}\right) dN_1 = 0 \tag{2.6}$$

If the combined system is in equilibrium there should be no change in the internal energy, hence $dU = 0$. The above expression thus defines constraints for when two systems are in equilibrium. Since the partial derivatives are important in determining equilibrium, we give them special names

$$\begin{aligned} \frac{\partial U_1}{\partial S_1} &= \frac{\partial U_2}{\partial S_2} \rightarrow \frac{\partial U}{\partial S} = \text{Temperature, } T \\ \frac{\partial U_1}{\partial V_1} &= \frac{\partial U_2}{\partial V_2} \rightarrow -\frac{\partial U}{\partial V} = \text{Pressure, } P \\ \frac{\partial U_1}{\partial N_1} &= \frac{\partial U_2}{\partial N_2} \rightarrow \frac{\partial U}{\partial N} = \text{Chemical potential, } \mu \end{aligned} \tag{2.7}$$

Notice that since we are dividing changes in extensive variables, all these variables describe intensive properties. From the above equation we can also identify three different types of equilibrium. Namely a *thermal equilibrium* due to flow of heat, which is determined by T, a *mechanical equilibrium* due to changes in the volume, determined by P and a *chemical equilibrium* due to flow of matter, determined by μ. This further cements the notion of intensive properties as forces and extensive properties as coordinates. For instance a difference in temperature gives rise to a force which drives a change in the entropy. Note that in our derivation we assumed that the total N, V and U were all constant. For other macroscopic constraints, similar definitions of the intensive variables are found. Some implications of equilibrium in simulations are discussed in note 2.2

Note 2.2. Equilibrium

According to statistical thermodynamics, a probability can be assigned to each available microstate in phase space. If we were to follow the evolution of a system long enough, this (equilibrium) probability distribution of the microstates would be recovered. This is independent of the starting configuration, since if the system started in a low probability region, this region would still be revisited with the correct probability. That means, that as soon as we specify a macrostate, we have assumed that the system is in equilibrium, since the accessible phase space volume is determined by the macrostate. In one way this might seem trivial, since thermodynamics describes systems in equilibrium, and ensembles, or macrostates, is a concept which is invented by thermodynamics.
In statistical thermodynamics we are often in need of a surrounding system, with constant N, V and E, of near infinite size, which we often take to be the universe. Since we defined the macrostate of the universe, statistical thermodynamics would tell us that the universe is in equilibrium. Although we can observe an increase in entropy (an increase in the "volume" of the universe), this increase is local, meaning that it is part of fluctuations around an equilibrium value.
This is, however, not an argument for the universe being in equilibrium. Thermodynamics is in fact in some ways a very practical theory, and was designed as one, and hence not designed for these types of questions.

2.3 The first laws of thermodynamics and the fundamental equation

We have seen that the entropy gives us clues about how a system evolves when N, V and E are kept constant. In the following sections other properties are derived, under different macroscopic constraints, which play the role of the entropy. We start from the first and second laws of thermodynamics. The first law of thermodynamics states that the change in internal energy, dU, is the sum of the heat added to the system, δq, the work done on the system, δw, and the change in energy due to a change in the amount of matter in the system (the number of particles in our case), dU_m.

The first law of thermodynamics

$$dU = \delta q + \delta w + dU_m \tag{2.8}$$

where δ is used to indicate a small quantity. This is commonly translated to conser-

vation of energy; Energy can never be destroyed or created, only converted between different forms.

The second law of thermodynamics states that the change in entropy is larger than, or equal, to the added heat divided by temperature, plus the change in entropy due to the change in matter.

The second law of thermodynamics

$$dS \geq \frac{\delta q}{T} + dS_m \tag{2.9}$$

where dS_m is the change in entropy due to exchanging matter. Note that the above form of the second law only holds for a reversible process. A common translation is that the entropy in an isolated system can never decrease. The second law of thermodynamics is statistical, meaning that from a macroscopic view, it would appear as if the entropy always increased. From a microscopic view however, there are fluctuations which also decrease the entropy.

Using eqs. 2.8 and 2.9, it is possible to find the total differential for the internal energy[8], $U(S, V, N)$ (which we have in fact already seen in eq. 2.6)

$$dU = TdS - pdV + \sum_i \mu_i dN_i \tag{2.10}$$

Eq. 2.10 is fundamental to thermodynamics, and will be used in the following section to derive the free energy.

2.4 The free energy

For a system of constant NVE we can make predictions about the direction which the system will evolve, based solely on the entropy. This was due to the equal probability of all states, which was due to that we held the energy constant. What about when the states do not have equal probability, i.e when the energy is not constant? In such cases one can not simply say that the entropy is maximized at equilibrium.

To further explore this, consider a box of volume V with rigid walls confining a number of particles N. We denote this box and it's content as $\mathcal{S}$ and refer to it as *the system*. $\mathcal{S}$ is surrounded by a much larger volume, which we simply call *the surrounding*, and denote as $\mathcal{S}'$. The energy of the combined system (system plus surrounding), E_T, is constant, $E_T = E_\mathcal{S} + E_{\mathcal{S}'}$. The system and surrounding cannot exchange particles but are in thermal contact with each other and heat can flow from the system to the surrounding and vice versa. Since we only concern ourselves with what happens at

equilibrium, we assume that the system is in thermal equilibrium with the surrounding. The temperature of the surrounding, $T_{\mathcal{S}'}$, is therefore equal to the temperature of the system, $T_{\mathcal{S}}$, according to eq. 2.6. Since the temperatures are equal, $T_{\mathcal{S}}$ and $T_{\mathcal{S}'}$ will be referred to simply as T. Therefore, in this setup, the number of particles $N_{\mathcal{S}}$, volume $V_{\mathcal{S}}$ and temperature $T_{\mathcal{S}}$ is constant in $\mathcal{S}$. From the previous section we know that the total entropy, S_T, will be maximized at equilibrium. Hence our goal is to find an expression for the total entropy, as a function of the properties of the system.

The total entropy change is the sum of the change in the system, and the change in the surrounding. We thus have for the entropy and energy

$$dS_T = dS_{\mathcal{S}} + dS_{\mathcal{S}'} \tag{2.11}$$

and

$$dU_T = dU_{\mathcal{S}} + dU_{\mathcal{S}'} = 0 \tag{2.12}$$

where dU_T is a change in the total energy, $dU_{\mathcal{S}}$ and $dU_{\mathcal{S}'}$ are the changes in energy in the system and the surrounding respectively. Since the surrounding has constant volume and constant number of particles, eq. 2.10 reads:

$$dU_{\mathcal{S}'} = TdS_{\mathcal{S}'} \rightarrow dS_{\mathcal{S}'} = \frac{dU_{\mathcal{S}'}}{T} \tag{2.13}$$

The total energy is constant and hence the change in energy in the system must equal an equal negative change in the surrounding, $dU_{\mathcal{S}} = -dU_{\mathcal{S}'}$. Substituting this relation into the above equation one get

$$dS_{\mathcal{S}'} = -\frac{dU_{\mathcal{S}}}{T} \tag{2.14}$$

Finally substituting eq. 2.14 into eq. 2.11 one arrives at

$$-TdS_T = dU_{\mathcal{S}} - TdS_{\mathcal{S}} \tag{2.15}$$

Eq. 2.15 relates a change in the total entropy, to changes in properties of the system, namely the energy and the entropy. Hence we can use this equation to predict the evolution of a system where N, V and T are constant. According to eq. 2.15, there exists a function, F, such that

$$F = U - TS \tag{2.16}$$

which, if the temperature is constant (so that $SdT = 0$), has a differential which is equal to eq. 2.15. We define the above function F as the *Helmholtz free energy*. Note that this expression assumes that the total system is in equilibrium. Now if we compare two different sets of microstates, their free energy difference gives us a way

to calculate which of these two sets that has the highest probability of being observed, thus the free energy determines the direction in which a system on average will evolve. Equally important is that the absolute free energy of a system is a way to quantify correlations between the particles. Hence the free energy is a very important tool in theoretical chemistry.

One thing that remains to be determined, is how the entropy can be calculated in a system such as the one described above (i.e when the energy, $U_{\mathcal{S}}$, is not constant). One thing we can do is to calculate the average Boltzmann entropy of our system. This is equal to averaging the entropy of each of the possible energy levels in our macrostate.

$$S = \sum_i p(U_i)S(U_i) = \sum_i p(U_i)k\ln\left(\Omega(U_i)\right) = -k\sum_i p(U_i)\ln\left(p(U_i)\right) \tag{2.17}$$

This expression is called *Gibbs entropy*, and will be used in the upcoming sections.

2.5 Statistical thermodynamics and the thermodynamic ensembles

While thermodynamics mainly describe macroscopic systems, *statistical thermodynamics* relates the thermodynamic observables to averages over the microstates. This corresponds to what is measured in most experiments. It is statistical thermodynamics one uses to calculate properties from molecular simulation. So the discussion about entropy in a previous section, could be regarded as stated from a statistical thermodynamical point of view.

So far we have looked at two special types of systems, where the number of particles N, volume V and the energy U or temperature T are constant. We say that such a set of constraints constitute a *macrostate*. A macrostate completely determines the accessible microstates, or equivalently the available volume in phase space. The collection of all accessible microstates, corresponding to some macrostate, is called an *ensemble*. In other words a macrostate can be considered as a type of equilibrium, and the population of the microstates follow the probability distribution corresponding to the macrostate. We will see later that this probability distribution is fundamental when running simulations of molecular systems.

The canonical ensemble (N,V,T)

Let us now revisit the example from the previous section, where a system $\mathcal{S}$ is surrounded by a much larger surrounding $\mathcal{S}'$. Lets further denote a specific microstate i in $\mathcal{S}$ as $\mathcal{S}_i$, and a microstate in $\mathcal{S}'$ as $\mathcal{S}'_i$. As before the combined system has constant

energy. The energy of the system and the surrounding are functions of the respective microstates, such that we have $U = U(\mathcal{S}) + U(\mathcal{S}')$.

Lets assume that the energy of the system is $U(\mathcal{S}_i) = \epsilon$, which means that the energy of the surrounding is $U - \epsilon$. Lets also assume for simplicity that the particles are distinguishable, so that we can leave out the factor $\frac{1}{N!}$ when calculating the number of states. For every accessible microstate, $\mathcal{S}_i$, of the system consistent with an energy ϵ, the surrounding can be in $\Omega(U - \epsilon)$ different states. Hence the probability of $\mathcal{S}$ to have an energy ϵ is

$$p(\epsilon) = \frac{\Omega(\epsilon)\Omega(U-\epsilon)}{\sum_i \Omega(\epsilon_i)\Omega(E-\epsilon_i))} = \frac{\exp\left[\frac{1}{k}S(\epsilon)\right]\exp\left[\frac{1}{k}S(U-\epsilon)\right]}{\sum_i \exp\left[\frac{1}{k}S(\epsilon_i)\right]\exp\left[\frac{1}{k}S(U-\epsilon_i)\right]} \tag{2.18}$$

where $\Omega(U - \epsilon)$ is the number of microstates of the surrounding with energy $U - \epsilon$, and $S(U - \epsilon)$ is the entropy of the surroundings. The sum in the denominator is taken over the energy levels available to the system. We now set $x = U - \epsilon$ and expand the entropy of the surrounding, $S(x) = k \ln[\Omega(x)]$, as a Taylor series. Since $\mathcal{S}'$ is assumed to be much larger that $\mathcal{S}$, it is clear that $U >> \epsilon$, and we can expand around $x' = U$. This means that we assume that the surrounding is infinitely large. The Taylor expansion is

$$S(x) = S(x') + \left[\frac{\partial S(x)}{\partial x}\right]_{x=x'}(x - x') + \mathcal{O}((x - x')^2) \tag{2.19}$$

where $\mathcal{O}(x'^2)$ is used to collect all terms of higher order than one. Since the volume of both the system and the surrounding are constant, no work can be performed. According the the first law of thermodynamics, eq. 2.8, the change in energy is then solely due to transfer of heat, $dU = \partial q$. The second law of thermodynamics, eq. 2.9, therefore reads $\frac{dS}{dU} = \frac{1}{T}$, which is the second term in the Taylor expansion in eq. 2.19. What remains is to calculate the rest terms in $\mathcal{O}((x - x')^2)$.

Since the temperatures of the system and surrounding are equal, we set $T_{\mathcal{S}} = T_{\mathcal{S}'} = T$. For the $\mathcal{O}((x - x')^2)$ terms one can then factor out a term

$$\frac{\partial^2 S}{\partial U^2} = \frac{\partial T^{-1}}{\partial U} = -\frac{1}{T^2}\frac{\partial T}{\partial U}$$

which goes to zero in the limit of an infinite system (it requires an infinite amount of energy to raise the temperature of such a system, i.e the heat capacity goes to infinity). Hence all terms of higher order than one disappears.

Substituting eq. 2.19 into eq. 2.18, one has eliminated the dependence on the surrounding, and the probability is now only a function of the energy and entropy of the

system

$$p(\epsilon) = \frac{\exp\left(\frac{1}{k}(S(\epsilon) - \frac{1}{T}\epsilon)\right)}{\sum_i \exp\left(\frac{1}{k}(S(\epsilon_i) - \frac{1}{T}\epsilon_i)\right)}$$

The probability can also be written as a function of the microstate, which further eliminates the dependence on the entropy. By noting that $\exp\left(\frac{1}{k}S(\epsilon)\right) = \Omega(\epsilon)$ is simply the degeneracy of energy level ϵ one arrives at

$$p(\mathcal{S}_i) = \frac{\exp\left(-\frac{1}{k_B T}U(\mathcal{S}_i)\right)}{\sum_{j\in\mathcal{S}} \exp\left(-\frac{1}{k_B T}U(\mathcal{S}_j)\right)}$$

where the sum in the denominator is now taken over the accessible microstates. The expression in the denominator is very important in statistical thermodynamics, and is called the *canonical partition function*, denoted Q. To see why it is important, we substitute the above expression into the Gibbs entropy, eq. 2.17

$$S = -k\sum_i \frac{\exp\left(-\frac{1}{k_B T}U_i\right)}{Q} \ln\left(\frac{\exp\left(-\frac{1}{k_B T}U_i\right)}{Q}\right) =$$

$$k\sum_i \frac{\exp\left(-\frac{1}{k_B T}U_i\right)}{Q}\left(\frac{1}{k_B T}U_i\right) + \ln(Q) =$$

$$\frac{1}{T}U + \ln(Q)$$

Substituting this result into eq. 2.15, we get

$$F = -k_B T \ln(Q) \text{ or equivalently } Q = e^{-\frac{1}{k_B T}F}$$

Hence the canonical partition function is related to the Helmholtz free energy. This, in turn, means that from Q, we can derive any other thermodynamic property.

As mentioned in an earlier chapter, from a classical point of view, space is continuous. This means that the sum in the partition function can be approximated as an integral.

$$Q = \sum_i \exp\left(-\frac{1}{k_B T}U_i\right) \approx \frac{1}{h^{3N}}\int_{\mathcal{S}} \exp\left(-\frac{1}{k_B T}U\left(\mathbf{r}^N, \mathbf{p}^N\right)\right) d\mathbf{r}^N d\mathbf{p}^N$$

where we have explicitly indicated that the energy depends on the two constituents of $\mathcal{S}_i$, namely the positions $\mathbf{r}^N$, and momenta $\mathbf{p}^N$ of the particles. Here one once again need to introduce Planck's constant into the volume element in the integral, to take into account the discretization of space from quantum mechanics

Unfortunately, direct calculation of the partition function is limited to very simple systems. In order to alleviate the problem, the energy, U, can be factored into two separate contributions; one for the potential energy, U_P, resulting from interactions and the other due to kinetic energies, U_K, $U = U_P + U_K$. Since the potential energy only depends on the position of the particles, and the kinetic energy only depends on the momentum. The partition function then reads

$$Q = \underbrace{\frac{1}{h^{3N}} \int_{\mathcal{S}} \exp\left(-\frac{1}{k_B T} K(\mathbf{p}^N)\right) d\mathbf{p}^N}_{Q_K} \underbrace{\int_{\mathcal{S}} \exp\left(-\frac{1}{k_B T} U(\mathbf{r}^N)\right) d\mathbf{r}^N}_{Q_U},$$

where Q_U is often denoted as the *configurational* partition function. The kinetic part of the partition function, Q_K, can be calculated analytically

$$\begin{aligned} Q_K = \frac{1}{h^{3N}} \int_{-\infty}^{\infty} \exp\left(-\frac{1}{k_B T} \sum_{i=0}^{N} \frac{|\mathbf{p}_i|^2}{2m_i}\right) d\mathbf{p}^N = \\ \prod_{i=0}^{N} \frac{1}{h^3} \int_{-\infty}^{\infty} \exp\left(-\frac{1}{k_B T} \frac{|\mathbf{p}_i|^2}{2m_i}\right) d\mathbf{p}_i = \prod_{i=0}^{N} \frac{1}{h^3} \left(2\pi m_i k_B T\right)^{\frac{3}{2}}, \end{aligned} \tag{2.20}$$

and thus reduces to a constant, at constant T. The factor 3 in the exponent in the final expression originates from the fact that we are integrating in all three dimensions for each particle. Eq. 2.20 is often reformulated in terms of the de Broglie wavelength $\Lambda = \frac{h}{\sqrt{2\pi m k_B T}}$. The canonical partition function then reduces to

$$Q = \frac{1}{\Lambda^{3N}} \int_{\mathcal{S}} \exp\left(-\frac{1}{k_B T} U(\mathbf{r}^N)\right) d\mathbf{r}^N.$$

and the probability becomes

$$p(\mathbf{r}^N) = \frac{\exp\left(-\frac{1}{k_B T} U(\mathbf{r}^N)\right)}{Q} \tag{2.21}$$

Thus we can focus on particle positions, $\mathbf{r}^N$. In the remainder of this chapter we however stick to the sum over discrete states. At any time one wishes to go to a classical description, one can just switch the sum to an integral and divide by h^{3N}, hence our choice has no impact of the actual results.

The grand-canonical ensemble (μ,V,T)

We now look at a different type of system. Consider, as in the previous section, a system embedded in a much larger surrounding. The total energy of the system plus surrounding is still constant, however, now we also allow the systems to exchange

particles. Hence the total number of particles is constant, but the number of particles in each of the two systems varies. We have seen that in such a system the chemical potential is same same for the two systems at equilibrium, eq. 2.6. Hence the number of microstates in the smaller system is now dependent on both the energy $U(\mathcal{S})$ and the number of particles $N(\mathcal{S})$. Note that the phase space of $\mathcal{S}$ now includes an additional coordinate, which is the number of particles. Proceeding as in the previous case, but this time directly writing the probability as a function of the microstate, the probability of observing a microstate in the smaller system is

$$p(\mathcal{S}_i) = \frac{\exp\left[\frac{1}{k}S(U - U(\mathcal{S}_i), N - N(\mathcal{S}_i))\right]}{\sum_j \exp\left[\frac{1}{k}S(U - U(\mathcal{S}_j), N - N(\mathcal{S}_j))\right]} \tag{2.22}$$

where the sum is over available microstates. We now use a 2-dimensional Taylor expansion of the entropy, and set $x = U - \epsilon$ and $y = N - n$ and expand around the point $(x' = U, y' = N)$. As in the previous case this is equivalent of assuming that the surrounding is infinitely large. The Taylor expansion reads

$$S(x,y) = S(x',y') - \frac{\partial S(x,y)}{\partial x}(x - x') - \frac{\partial S(x,y)}{\partial y}(y - y') + \\ \mathcal{O}\left((x - x')^2\right) + \mathcal{O}\left((y - y')^2\right)$$

where again $\frac{dS(U-\epsilon,N-n)}{dU_{S'}} = \frac{1}{T_{S'}}$ and from eq. 2.7 we get $\frac{dS(U-\epsilon,N-n)}{dN_{S'}} = -\frac{\mu_{S'}}{T}$. The system is in equilibrium with the surrounding and hence $T = T_S = T_{S'}$ and $\mu = \mu_S = \mu_{S'}$. Substituting these results into eq. 2.22 we arrive at

$$P(\epsilon, n) = \frac{\exp\left[\frac{1}{k_B T}\left(\mu n - \epsilon\right)\right]}{\sum_i \exp\left[\frac{1}{k_B T}\left(\mu N(\mathcal{S}_i) - U(\mathcal{S}_i)\right)\right]} \tag{2.23}$$

In the same way as before, we can identify the expression in the denominator as the grand canonical partition function:

$$\Xi = \sum_i \exp\left[\frac{1}{k_B T}\left(\mu N(\mathcal{S}_i) - U(\mathcal{S}_i)\right)\right]$$

In section 2.4 we derived the Helmholtz free energy for a system where N, V and T are constant. Following the same procedure while no longer keeping N constant, one ends up with a free energy differential,

$$-T dS_{total} = dU - T dS + \mu dN$$

Which then yields another free energy, called the Grand potential

$$\Phi = U - TS + \mu N$$

Just as in the case of the canonical partition function, the grand canonical partition function is related to this free energy through

$$-k_B T \ln(\Xi) = \Phi$$

In papers II-VI we make use of the grand canonical ensemble to simulate our systems. In paper III we directly calculate the grand potential using a method called classical density functional theory, which will be introduced in another chapter.

2.6 Energy, entropy and the discretization of space

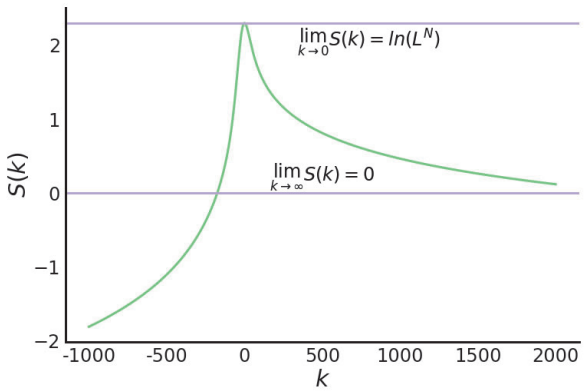

Figure 2.4: Illustration of the entropy in a one dimensional system, consisting of one particle in an external field, defined by $\phi(x) = kx^2$. The entropy is here plotted against the force constant k. The purple lines shows the relevant limits.

Before ending this chapter, we will in this section investigate a simple theoretical system. In this example the entropy is analytically available, which enables us to highlight some interesting aspects about the interplay between energy and entropy, as well as the effect of going from a quantized space (as in quantum mechanics) to a continuous space (as in classical mechanics).

Consider a single particle on a line of length L. An external potential is acting along the line and has the form $\phi(x) = kx^2$, where k is a force constant and x is a position on line. When $k = 0$, the system is equivalent to an ideal particle on a line. The (configurational) partition function of this system is

$$Q = \int_{L/2}^{L/2} e^{-\frac{1}{T}kx^2} dx$$

where we have set $k_B = 1$ and $h = 1$ for simplicity. In this system one would expect that as $k \to \infty$, the entropy would go towards 0, since only one state is then available

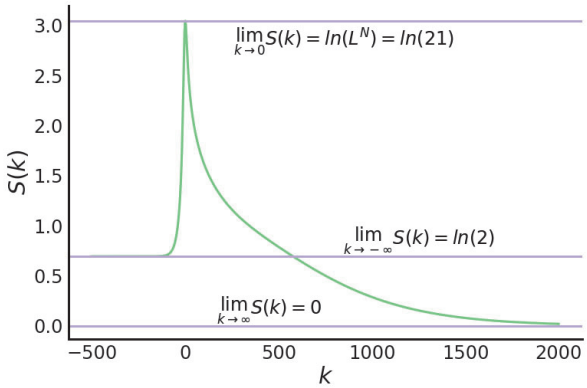

Figure 2.5: Illustration of the entropy in a one dimensional system, consisting of one particle in an external field, defined by $\phi(x) = kx^2$. The entropy is here plotted against the force constant k. The purple lines shows the relevant limits.

(in the middle of the line). As $k \to -\infty$ one would expect an entropy of $\ln(2)$, since two states are available, one on each side of the endpoints. When $k \to 0$ one expects that the entropy is equal to that of an ideal particle, $\ln(L^N)$.

As we have seen before the free energy is given by $F = -k_B T \ln(Q)$ and the entropy is given by $S = -\frac{\partial F}{\partial T}$. To simplify the algebra when calculating the entropy, we define

$$\gamma = \sqrt{\frac{k}{T}} \text{ and } \omega = \sqrt{\pi}\,\mathrm{erf}\left(\gamma\frac{L}{2}\right)$$

The entropy is then given by

$$S = -N\left(Le^{-\frac{L^2}{4}\gamma^2}\gamma - \omega - 2\omega\ln\left(\frac{\omega}{\gamma}\right)\right)$$

A plot of the entropy as a function of the force constant, k is shown in figure 2.4. In this figure the limits are also shown. This entropy displays the correct limiting behaviour in the limit $k \to \infty$, as well as when $k \to 0$. In the latter case, the entropy tends to that of an ideal particle, which is also a global maximum, as can be seen in fig. 2.4. As a side note this is equivalent to the limit of infinite temperature, which is also readily seen from the Boltzmann factor. In the limit $k \to -\infty$ the entropy does not show the correct behaviour. This is due to the approximation of going from a discrete space to a continuous space. Instead calculating the entropy in a discrete space yields an entropy as plotted in fig. 2.5, which has the correct limits. This procedure amounts to dividing the line into $\mathcal{L}$ segments, then summing over those segments in

the partition function. If we set $dx = \frac{L}{\mathcal{L}}$, the partition function can be written as

$$Q_D = \sum_{x=0}^{\mathcal{L}-1} \exp\left[-\frac{1}{T}k\left(L\left(\frac{1}{\mathcal{L}+1} - \frac{1}{2}\right) + xdx\right)^2\right] \tag{2.24}$$

where the subscript "D" on the partition function denotes that it is calculated over a discretized space. One can then use Gibbs formula in eq. 2.17, to calculate the entropy, and then plot it as a function of the force constant.

Chapter 3

Energy

We have now arrived at the second main thermodynamic property: Energy. As we saw in the previous chapter, energy, together with entropy, constitute the free energy. The energy introduced here, the *interaction energy* (which is in the remainder of this chapter simply referred to as energy), is a way to quantify the correlations between particles, that are not due to entropy. There is a constant interplay between energy and entropy, and more often than not, they result in opposing forces. In fact, one could even argue that they always are opposing forces, as introducing interactions (i.e adding energy to the system) *always* decreases the entropy in a system.

3.1 Electrostatic interactions

There are many different types of interactions between particles, and they can be very complex. For instance the polarization of an atom in the presence of another atom. While the first atom is polarized, its new charge distribution will in turn polarize the second, or a third atom, which will then again affect the first atom. Such interactions would have to be solved iteratively. One simplification we can make is that all of the interactions are pairwise and pairwise additive.

In this thesis we will only concern ourselves with two types of interactions. One due to the excluded volume of particles (specifically Pauli repulsion), the second which originate from the correlations between charges, i.e electrons and protons, which is the focus of this chapter. This type of interactions are called electric interactions. In reality particles interact via different mechanisms, many deriving from electric interactions (Keesom, London, Debye etc). In classical molecular simulations it is common to assume that electric interactions occur statically, namely that the interactions do not depend on the movement of the charges, which brings us to *electrostatic* interactions,

which will be the focus of this chapter. In addition to statically occurring interactions, we assume that all charges are infinitesimal points in space. In this regime, two charged particles i and j with charges q_i and q_j, can be represented by two delta functions, $\rho(\mathbf{r}) = q_i\delta(|\mathbf{r}_i - \mathbf{r}|) + q_j\delta(|\mathbf{r}_j - \mathbf{r}|)$, where $\mathbf{r}_i$ is the position of the i point charge. q is thus defined as the valency times the elemental charge. The potential generated by these two point charges is given by Poisson's equation.

Poisson's equation

Poisson's equation has a central role in electrostatics since it relates the electric potential, $\phi(\mathbf{r})$, to the generating charge distribution, $\rho(\mathbf{r})$.

$$\nabla \cdot [\epsilon_0\epsilon(\mathbf{r}, T)\nabla\phi(\mathbf{r})] = -\rho(\mathbf{r}),$$

where $\epsilon(\mathbf{r}, T)$ is a function describing the relative electric permittivity of the medium and ϵ_0 is the permittivity of free space. Often one assumes homogeneous permittivity of the medium, $\epsilon(\mathbf{r}, T) = \epsilon_r(T)$, in which case one can write $\epsilon_0\epsilon_r(T) = \epsilon(T)$. Poisson's equation is then reduced to:

$$\Delta\phi(\mathbf{r}) = -\frac{\rho(\mathbf{r})}{\epsilon(T)}, \tag{3.1}$$

where $\Delta = \nabla \cdot \nabla = \left[\frac{\partial^2}{\partial x^2} + \frac{\partial^2}{\partial y^2} + \frac{\partial^2}{\partial z^2}\right]$ is the Laplace operator. If we go back to the example of two point charges, the solution to Poisson's equation, the potential, is[9]

$$\phi(\mathbf{r}) = \frac{1}{4\pi\epsilon(T)}\left(\frac{q_i}{|\mathbf{r} - \mathbf{r}_i|} + \frac{q_j}{|\mathbf{r} - \mathbf{r}_j|}\right)$$

The interaction energy between two point charges i and j is thus

$$U_{ij}(r) = \frac{q_i q_j}{4\pi\epsilon(T)r_{ij}}$$

where r_{ij} is the distance between the charges and $\epsilon(T)$ is the dielectric permittivity of the medium intervening the two charges at temperature T. This potential is called the Coulomb potential. To be a bit more precise the Coulomb potential is actually a free energy, due to the fact that the dielectric permittivity depends on the temperature. It thus includes an entropy component, and not just an energy component. This entropy component comes from the response of the solvent, to the presence of the two charges q_i and q_j.

Since the Coulomb energy decays as r^{-1}, we say that it is long ranged. This means that for two particles that are relatively far away from each other, there is still a non negligible interaction energy. Hence, as stated in the introduction, we need to introduce PBC. Before diving too deep into how to solve this, lets define what we mean with *energy* in the context of simulations.

3.2 Energy of a simulation box

Consider a general system composed of charged particles, and a number of replica systems, to approximate a bulk system. The total electrostatic (Coulomb) energy of this system is given by the familiar equation[6]:

$$U_S = \frac{1}{2}\frac{1}{4\pi\epsilon(T)}\sum_{\mathbf{n}}{}' \sum_i \sum_j q_i q_j \frac{1}{|(\mathbf{r}_i - \mathbf{r}_j) + \mathbf{n} \circ \mathbf{L}|} \tag{3.2}$$

where $\circ$ denotes the component-wise product and $\mathbf{L} = [L_x, L_y, L_z]$ is a vector describing the (orthogonal) box. The sum over $\mathbf{n} \in \mathbb{Z}^3$ runs over all replicas and the prime indicates that when $\mathbf{n} = \mathbf{0}$, the term $i = j$ is excluded. The factor $1/2$ in front is usually attributed to cancellation of double counting. A subtle (and perhaps a bit confusing) detail about the above equation, is that terms where $i = j$ and $\mathbf{n} \neq \mathbf{0}$ are only included once (for each n), yet still divided by two. Hence the factor $1/2$ is not only accounting for double counting, but as we shall see, also due to how the energy of the simulation box is defined (which perhaps one could argue is the same thing).

Consider a system $\mathcal{S}$, containing only two particles A and B, as well as one of its replicas $\mathcal{S}'$, as in fig. 3.1. We are interested in finding the energy of $\mathcal{S}$. One might be tempted to define the energy as simply the sum of the interactions of all particles in $\mathcal{S}$ with all other particles which, avoiding double counting, amounts to

$$U_{\mathcal{S}} = AB + AA' + AB' + BA' + BB'$$

The above equation however yields an energy that is not extensive, and hence is erroneous. Instead one defines the energy as the total energy, including the energy of all replicas and the interactions between them, divided by the number of replicas. The *total* energy of such a system is the sum of all interactions:

$$U_T = AB + AA' + AB' + BA' + BB' + A'B'$$

This equation can be simplified since $AB = A'B'$, due to symmetry. One then arrives at

$$U_T = 2AB + AA' + AB' + BA' + BB'$$

Dividing by 2 yields the energy per box (or equivalently the energy of $\mathcal{S}$) and thus we have:

$$U_{\mathcal{S}} = AB + \frac{1}{2}(AA' + AB' + BA' + BB')$$

If the minimum image convention is used (and we extend the system in fig. 3.1 with another replica to the left) we get that $AB' = BA'$, and the above equation can then be written as

$$U_{\mathcal{S}} = AB + AB' + \frac{1}{2}(AA' + BB')$$

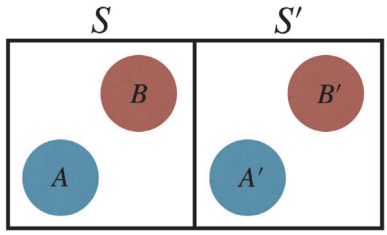

Figure 3.1: A simple illustration of a system and one replica

Hence for a general system $\mathcal{S}$ with an arbitrary number of replicas $\mathcal{S}'$, the energy can be written as in eq. 3.2.

3.3 Ewald summation

Charge-charge interactions are arguably the most important of the electrostatic inter-particle interactions in ionic systems. In such systems these interactions are sometimes one or more orders of magnitude stronger than other electrostatic interactions. Hence, it is often a reasonable approximation in ionic systems to neglect all other interactions, except exchange repulsion.

In simulations, the size of the systems that we are able to simulate are limited by the computational resources available. We also have to figure out how to handle the boundaries of the simulation box. A first approach to mitigate this problem and minimize size effects is to introduce PBC. Since electrostatic interactions are long ranged, simply using PBC with a minimum image truncation (defined above) is in many cases inadequate.

As mentioned earlier, the most common way of emulating an infinite system in molecular simulation, is to replicate the simulation box (fig. 1.1), and represent each charged by a point charge. The potential generated by such a charge distribution is given by:

$$\phi(\mathbf{r}) = \frac{1}{4\pi\epsilon(T)} \sum_{\mathbf{n}\in\mathbb{Z}^3}{}' \sum_{i=1}^{N} \frac{q_i}{|\mathbf{r} - \mathbf{r}_i + \mathbf{n} \circ \mathbf{L}|},$$

Direct summation of the box replicas yields a slowly converging sum due to the $|\mathbf{r}|^{-1}$ dependency. This sum is also conditionally convergent, and the result depends on the summation order (or geometry). To overcome the slow and conditionally converging sum, Ewald summation [10,11] is the predominantly used method. In Ewald summation, the infinite sum is split into two parts, one short-ranged and another long-ranged term. To achieve this, a screening charge distribution, $\varrho(\mathbf{r})$, is added and subtracted from the original charge distribution (see fig. 3.2), which we here assume to be a collection

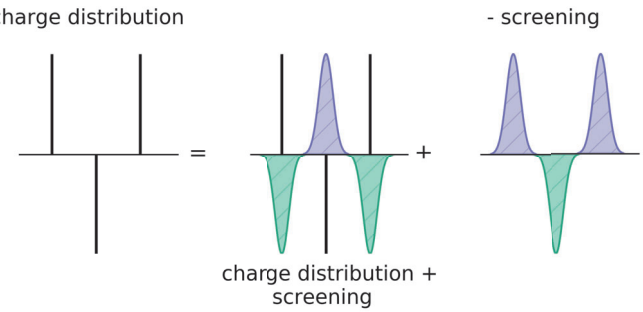

Figure 3.2: Illustration of eq. 3.3. purple and green distributions symbolize $\varrho(\mathbf{r})$ and $-\varrho(\mathbf{r})$ respectively. Black lines represent the delta functions. Note that the scale is not accurate

of point charges, $q\delta(\mathbf{r})$:

$$\rho(\mathbf{r}) = \underbrace{\sum_{i=1}^{N} q_i \delta(\mathbf{r}-\mathbf{r}_i) - \sum_{i=1}^{N} q_i \varrho(\mathbf{r}-\mathbf{r}_i)}_{\rho_S(\mathbf{r})} + \underbrace{\sum_{i=1}^{N} q_i \varrho(\mathbf{r}-\mathbf{r}_i)}_{\rho_L(\mathbf{r})}. \tag{3.3}$$

A common screening charge distribution is in the form of Gaussian functions:

$$\varrho(\mathbf{r}) = \frac{1}{(2\pi\sigma^2)^{3/2}} e^{-\frac{|\mathbf{r}|^2}{2\sigma^2}}, \tag{3.4}$$

where σ is the standard deviation of the Gaussian. σ is related to the so called "splitting parameter", α, by $\alpha = \frac{1}{\sqrt{2}\sigma}$. Since we have added and subtracted $\varrho(\mathbf{r})$, the resulting charge distribution is effectively split into one short-range, $\rho_S(\mathbf{r})$, and one long-range term, $\rho_L(\mathbf{r})$. As we will see later, the decay of the resulting potential is dependent on σ. The potential generated by a charge distribution is given by Poisson's equation, eq. 3.1 and, due to linearity, the short- and long-range parts can be solved separately. The short-ranged potential is given directly as a solution:

$$\Delta\phi_S(\mathbf{r}) = -\frac{1}{\epsilon(T)}\rho_S(\mathbf{r}) \rightarrow$$

$$\phi_S(\mathbf{r}) = \frac{1}{4\pi\epsilon(T)} \sum_{\mathbf{n}\in\mathbb{Z}^3} \sum_{i=1}^{N} q_i \frac{\operatorname{erfc}\left(\frac{1}{\sqrt{2}\sigma}|\mathbf{r}-\mathbf{r}_i+\mathbf{n}\circ\mathbf{L}|\right)}{|\mathbf{r}-\mathbf{r}_i+\mathbf{n}\circ\mathbf{L}|}, \tag{3.5}$$

which converges rapidly for large $|\mathbf{r}-\mathbf{r}_i|$. It is common to use a minimum image truncation for the short range potential, since σ can be chosen so that the magnitude of potential is very small at the cutoff. The interaction energy resulting from the short range potential is thus given by:

$$U_S = \frac{1}{2}\sum_{j=1}^{N} q_j \phi'_S(\mathbf{r}_j) \tag{3.6}$$

where the prime on ϕ_S (given by eq. 3.5) indicate that when $|\mathbf{n}| = 0$, the term $\mathbf{r}_i = \mathbf{r}_j$ is excluded.

Solving for the long-ranged part however, yields a slowly converging sum

$$\phi_L(\mathbf{r}) = \frac{1}{4\pi\epsilon(T)} \sum_{\mathbf{n}\in\mathbb{Z}^3} \sum_{i=1}^{N} q_i \frac{\operatorname{erf}\left(\frac{1}{\sqrt{2}\sigma}|\mathbf{r} - \mathbf{r}_i + \mathbf{n}\circ\mathbf{L}|\right)}{|\mathbf{r} - \mathbf{r}_i + \mathbf{n}\circ\mathbf{L}|}, \tag{3.7}$$

due to the $\operatorname{erf}(\mathbf{r})$ term. To alleviate this problem, the long ranged potential is instead solved in Fourier space. This method involves expanding the long range potential as a complex Fourier series

$$\phi_L(\mathbf{r}) = \frac{1}{V} \sum_{\mathbf{k}} \tilde{\phi}_L(\mathbf{k}) e^{i\mathbf{k}\cdot\mathbf{r}}, \tag{3.8}$$

where $\mathbf{k} = (2\pi/L_x, 2\pi/L_y, 2\pi/L_z) \circ \mathbf{n}$ are the reciprocal wave vectors, $\circ$ again denotes a component-wise product and V is the volume of the simulation box. Using Poisson's equation (eq. 3.1) in Fourier space, $\tilde{\phi}(\mathbf{k}) = \frac{\tilde{\rho}(\mathbf{k})}{k^2\epsilon(T)}$, where $k = |\mathbf{k}|$ eq. 3.8 can be rewritten as:

$$\phi_L(\mathbf{r}) = \frac{1}{V} \sum_{\mathbf{k}} \frac{\tilde{\rho}_L(\mathbf{k})}{k^2\epsilon(T)} e^{i\mathbf{k}\cdot\mathbf{r}}. \tag{3.9}$$

Hence one needs to calculate the Fourier transform of the long range charge distribution $\rho_L(\mathbf{k})$, which is given as:

$$\tilde{\rho}_L(\mathbf{k}) = \frac{1}{(2\pi\sigma^2)^{3/2}} \sum_{\mathbf{n}\in\mathbb{Z}^3} \sum_{j=1}^{N} q_j \int_V e^{-i\mathbf{k}\cdot\mathbf{r}} e^{-\frac{|\mathbf{r}-\mathbf{r}_j+\mathbf{n}\mathbf{L}|^2}{2\sigma^2}} d^3\mathbf{r}.$$

Note that in eq. 3.6, the term $\mathbf{r}_i = \mathbf{r}_j$ when $|\mathbf{n}| = 0$ is removed, therefore the above equation should also exclude this term (a charge should not interact with it's own screening charge distribution). However, the above equation can be solved by making the variable substitution $\mathbf{r} + \mathbf{n}\circ\mathbf{L} \to \mathbf{r}$. Thus, by rearranging and multiplying with $1 = e^{ik\mathbf{r}_j} e^{-ik\mathbf{r}_j}$ one ends up with:

$$\tilde{\rho}_L(\mathbf{k}) = \sum_{j=1}^{N} e^{i\mathbf{k}\cdot\mathbf{r}_j} q_j \frac{1}{(2\pi\sigma^2)^{3/2}} \int_{\mathbb{R}^3} e^{-i\mathbf{k}\cdot(\mathbf{r}-\mathbf{r}_j)} e^{-\frac{|\mathbf{r}-\mathbf{r}_j|^2}{2\sigma^2}} d^3\mathbf{r}.$$

The term $\mathbf{r}_i = \mathbf{r}_j$ when $|\mathbf{n}| = 0$ is called the *self term* and will be removed later.

Using the Fourier transform of a Gaussian $e^{-\frac{x^2}{2\sigma^2}} \xrightarrow{\mathscr{F}} \sqrt{2\pi\sigma^2} e^{-\frac{\sigma^2 k^2}{2}}$, and the corresponding for the y and z dimensions, and substituting the result into eq. 3.9 yields

the long range potential in real space:

$$\phi_L(\mathbf{r}) = \frac{1}{V} \sum_{|\mathbf{k}|\neq 0} \sum_{j=1}^{N} q_j \frac{1}{k^2 \epsilon(T)} e^{i\mathbf{k}\cdot(\mathbf{r}-\mathbf{r}_j)} e^{-\frac{\sigma^2 k^2}{2}}. \tag{3.10}$$

The infinite sum over $\mathbf{k}$ is in practice limited using a cutoff, k_{max}, so that only terms where $k < k_{max}$ is included in the sum. The term where $k = 0$ is called the *surface term*[12], and has been excluded from the sum since it diverges. This term has to be calculated in another manner, which will be shown later.

Comparing eqs. 3.7 and 3.10 for the long range potential, eq. 3.10 scales as $\frac{1}{|\mathbf{k}|^2}$ which converges much faster than the $\frac{1}{|\mathbf{r}|}$ term in eq. 3.7. The resulting interaction energy for the long range potential is:

$$U_L = \frac{1}{2} \sum_{i=1}^{N} q_i \phi_L(\mathbf{r}_i) \tag{3.11}$$

We now have both the short and long range contributions to the energy. What remains is to calculate the two remaining contributions, the self energy and the surface energy:

The self term

As mentioned above one needs to remove the spurious interaction between a point charge and its own screening charge distribution (the self term). The self energy, resulting from the self term, is the potential at $\mathbf{r} = \mathbf{r}_i$ generated by a Gaussian charge distribution (eq. 3.7). By setting $\mathbf{r}_i = \mathbf{0}$ and letting $|\mathbf{r}| \to 0$

$$\phi_{self} = \phi_L(0) = \frac{1}{4\pi\epsilon(T)} \lim_{r\to 0} \frac{q}{r} \operatorname{erf}\left(\frac{1}{\sqrt{2}\sigma} r\right) = \frac{1}{4\pi\epsilon(T)} \frac{q\sqrt{2}}{\sqrt{\pi}\sigma} \to$$

$$U_{self} = \frac{1}{4\pi\epsilon(T)} \sum_{i=1}^{N} \frac{q_i^2}{\sqrt{2\pi}\sigma} \tag{3.12}$$

Hence the above term, U_{self}, needs to be subtracted from the total energy.

The surface term

As previously stated, when $\mathbf{k} = 0$ the expression in eq. 3.10 diverges. Hence one needs to calculate this term in another manner. This term is usually called the surface term. To calculate this contribution we follow the procedure of Hu[13], and start from the value of the long range energy as $\mathbf{k} \to 0$ (i.e eq 3.11)

$$\lim_{\mathbf{k}\to\mathbf{0}} U_L = U_{surf} = \frac{1}{V} \lim_{\mathbf{k}\to\mathbf{0}} \sum_{i=1}^{N} \sum_{j=1}^{N} q_i q_j \frac{e^{-\frac{\sigma^2|\mathbf{k}|^2}{2}} e^{i\mathbf{k}\cdot\mathbf{r}_{ij}}}{k^2}$$

where $\mathbf{0}$ is the zero vector $(0,0,0)$. The above expression diverges due to the k^2 term in the numerator. Therefore this equation is expanded as a geometric series

$$e^x = \sum_{n=0}^{\infty} \frac{x^n}{n!}$$

where if we set $x = -\frac{\sigma^2 k^2}{2} + i\mathbf{k}\cdot\mathbf{r}_{ij}$ one arrives at

$$U_{surf} = \frac{1}{V}\lim_{\mathbf{k}\to\mathbf{0}} \frac{1}{k^2} \sum_{i=1}^{N}\sum_{j=1}^{N} q_i q_j \left[1 - \frac{\sigma^2 k^2}{2} + i\mathbf{k}\cdot\mathbf{r}_{ij} + \frac{1}{2}\left(-\frac{\sigma^2 k^2}{2} + i\mathbf{k}\cdot\mathbf{r}_{ij}\right)^2\right] + \mathcal{O}(\mathbf{k^2})$$

All terms containing odd powers of $i\mathbf{k}\cdot\mathbf{r}_{ij}$ cancels because $\mathbf{r}_{ij} = -\mathbf{r}_{ji}$. Terms not dependent on $\mathbf{r}_{ij}$ also cancels due to electroneutrality. All terms containing k^3 or higher disappears as the limit is taken. Hence the only terms we are left with is

$$U_{surf} = -\frac{1}{2V}\lim_{\mathbf{k}\to\mathbf{0}} \sum_{i=1}^{N}\sum_{j=1}^{N} q_i q_j \frac{(\mathbf{k}\cdot\mathbf{r}_{ij})^2}{k^2} \tag{3.13}$$

Since $\mathbf{k}$ is a vector, one must choose a path when taking the limit. A natural first choice would be to let $k \to 0$, which would amount to transforming the above equation into spherical polar coordinates, then averaging out the angular parts of $\mathbf{k}$, k_θ and k_ϕ, before letting the radial component $k_r = |\mathbf{k}| = k$ go towards zero.

$$U_{surf} = -\frac{1}{2V}\lim_{k\to 0} \sum_{i=1}^{N}\sum_{j=1}^{N} q_i q_j \frac{\int_0^{2\pi}\int_0^{\pi} (\mathbf{k}\cdot\mathbf{r}_{ij})^2 \sin(k_\theta) dk_\theta dk_\phi}{k^2 \int_0^{2\pi}\int_0^{\pi} \sin(k_\phi) dk_\theta dk_\phi}$$

where denominator is simply equal to $\frac{1}{4\pi k^2}$. For notational simplicity, lets now denote $r_x = |r_{ij}|\cos(r_\phi)\sin(r_\theta)$, $r_y = |r_{ij}|\sin(r_\phi)\sin(r_\theta)$ and $r_z = |r_{ij}|\cos(r_\theta)$. After expanding the dot product in the square term, all cross terms disappear in the integration, and only the square terms survive.

$$\frac{1}{4\pi k^2}\int_0^{2\pi}\int_0^{\pi} (\mathbf{k}\cdot\mathbf{r}_{ij})^2 \sin(k_\theta) dk_\theta dk_\phi =$$
$$\frac{1}{4\pi} r_x^2 \int_0^{2\pi}\int_0^{\pi} \sin(k_\theta)(\cos(k_\phi)\sin(k_\theta))^2 dk_\theta dk_\phi +$$
$$\frac{1}{4\pi} r_y^2 \int_0^{2\pi}\int_0^{\pi} \sin(k_\theta)(\sin(k_\phi)\sin(k_\theta))^2 dk_\theta dk_\phi +$$
$$\frac{1}{4\pi} r_z^2 \int_0^{2\pi}\int_0^{\pi} \sin(k_\theta)(cos(k_\theta))^2 dk_\theta dk_\phi = \frac{r_{ij}^2}{3}$$

Since each of the above integrals are equal to $\frac{4\pi}{3}$. Using the definition of the dipole moment $\mathbf{M} = \sum_i^N q_i \mathbf{r}_i$ and substituting in this result into eq. 3.13 yields

$$U_{surf} = -\frac{1}{2V} \lim_{k\to 0} \sum_{i=1}^{N} \sum_{j=1}^{N} q_i q_j \frac{r_{ij}^2}{3} = \frac{2\pi}{3V} \mathbf{M} \cdot \mathbf{M} \tag{3.14}$$

where we have used $\sum_{i=1} \sum_{j=1} q_i q_j \mathbf{r}_{ij}^2 = -2 \left(\sum_i q_i \mathbf{r}_i\right)^2$, and the fact that the system is electroneutral. Using eq. 3.14 is equivalent to adopting a spherical summation geometry.

Another way to take the limit in eq. 3.13 is to first let $\mathbf{k}$ go to zero in the (x, y) plane and then in z. This is equivalent to adopting a slabwise summation geometry, and yields a surface term of the form:

$$\begin{aligned} -\frac{1}{2V} \sum_{i=1}^{N} \sum_{j=1}^{N} q_i q_j \lim_{k_z\to 0} \left(\lim_{k_{xy}\to 0} \frac{(\mathbf{k} \cdot \mathbf{r}_{ij})^2}{k^2} \right) = \\ -\frac{1}{2V} \sum_{i=1}^{N} \sum_{j=1}^{N} q_i q_j z_{ij}^2 = \frac{1}{V} M_z \end{aligned} \tag{3.15}$$

where M_z is the dipole moment in the z dimension. It has been shown that when simulating systems of slab geometry, the above surface term yields good results[14]. When simulating bulk systems, the spherical surface term if the most common[6].

Since $\mathbf{k}$ is has units of reciprocal length, $\mathbf{k} \to 0$ correspond to infinite distance. Therefore, one can argue that the surface term depends on the permittivity of the surrounding medium, $\epsilon(T)_{sur}$, i.e on the surface of the crystal, instead of the permittivity of the crystal itself. If so called tin foil boundary conditions are used, where the surrounding medium is assumed to be infinitely conducting ($\epsilon(T)_{sur} = \infty$), the surface term therefore vanishes. When simulating bulk systems containing ions, it is suggested to use tinfoil boundary conditions[10]. It remains to be determined in which cases this is indeed the best choice, or that simply the dipole moment squared is so small that it does not make any difference.

Now we are finally equipped with all terms necessary to calculate the energy using Ewald summation. Combining eqs. 3.6, 3.11, 3.12 and 3.14 yields the final expression for the total energy

$$U = U_S + U_L - U_{self} + U_{surf}.$$

Note that since we have assumed an electroneutral cell in the derivation above, this expression is only valid in electrically neutral systems. Although simulating systems with a net charge might yield correct results, the net charge can also introduce artifacts[15].

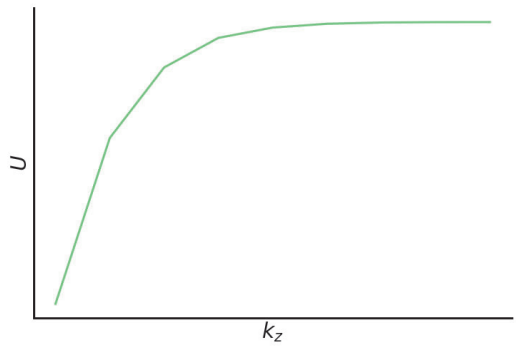

Figure 3.3: Plot of the energy vs the reciprocal cutoff value along z.

A lot of optimizations to Ewald summation exist in literature such as symmetry considerations of the trigonometric functions and the choice of parameters[16], as well as discretization of space and using fast Fourier transforms[17], especially in combination with interpolation[18]. Most popular simulation packages use some or a combination of these optimizations[19,20,21].

Practical considerations

How does one choose the different parameters when running an actual simulation? The accuracy of the real space term is obviously dependent on the real space cutoff, as well as the width of the gaussian screening function (σ). Choosing a value of $\frac{1}{\sqrt{2}\sigma} = \frac{\pi}{R_c}$, yields a value at the cutoff of

$$\frac{\operatorname{erfc}\left(\frac{\pi}{R_c}R_c\right)}{R_c} \approx \frac{10^{-5}}{R_c} \tag{3.16}$$

which is a reasonable choice for most cutoffs, and a good rule of thumb[22]. Choosing the reciprocal space cutoff is not as easy. In practice one has to calculate the energy of a random configuration, of the system of interest, for different values of the cutoff k_{max} and plot the result (as in fig. 3.3), to see when the energy converges to within a tolerable error. When using asymmetric simulation boxes, further considerations are needed. Consider the system in fig. 3.4. When a spherical cutoff is used, the volume outside the cutoff is larger in one of more dimensions compared to the other. This in turn means that more reciprocal vectors are needed in the longer dimension, since it requires more trigonometric functions to describe the fluctuations in the charge distribution. This can be a problem when simulating narrow slits. Then the number of reciprocal vectors in the large dimensions has to be much larger than in the short dimension.

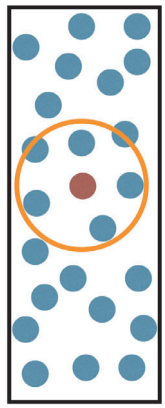

Figure 3.4: Illustration of an asymmetric simulation box. The figure shows the cutoff (orange circle) of a tagged particle (red).

3.4 Using alternative screening functions

As mentioned in the previous section, Ewald summation is the predominantly used method for calculating the electrostatic interactions in molecular simulation. The accuracy of energy evaluations using the Ewald summation technique depends on three parameters, namely the real space cutoff R, the standard deviation of the Gaussian screening charge distribution, σ, and the number of reciprocal wave vectors in the long range term k_{max} (see eq. 3.11). Changing σ alters the "effectiveness" of the screening charges and thus changes the value of the short range potential at the cutoff. In turn, this also changes the required k_{max} for a given accuracy. Thus decreasing σ results in a decrease of the value of the potential at the cutoff R, which in turn increases the required k_{max}. In practice σ is chosen so that the value of the factor $\frac{1}{\mathbf{r}}\,\mathrm{erfc}\,(\frac{1}{\sqrt{2}\sigma}\mathbf{r})$, in eq. 3.5, at the short range cutoff is small, usually on the order 10^{-6} to 10^{-5}. Then k_{max} is chosen large enough so that the reciprocal sum converges with a given accuracy. Thus there is a balance between R, σ and k_{max} which need fine tuning for optimal efficiency and accuracy, and the values depends on the system studied. This adds extra complexity as the effect of changing the parameters may not be apparent to an unexperienced user, as neither of the parameters has a direct relationship with the accuracy of the calculated energies or forces. It also not apparent why a Gaussian screening function is the optimal choice for general systems.

In paper I, entitled "An Exact Ewald Summation Method in Theory and Practice" we present the Ewald method with a different screening charge function, namely a truncated Gaussian. Since this function is spherically symmetric, it is convenient to

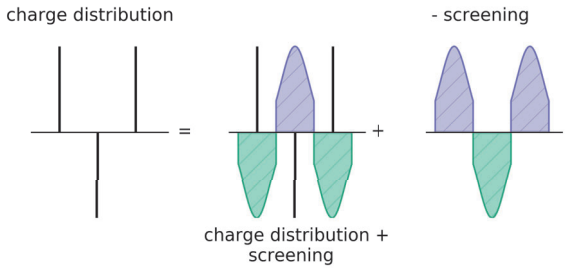

Figure 3.5: Illustration of the split in the charge distribution. Purple and green distributions symbolize the added and subtracted screening charge distributions. Black lines indicate the delta functions. Note that the scale is not accurate.

express it in spherical coordinates, $|\mathbf{r}| = r$:

$$\varrho_T(r) = \frac{\varrho(r)}{4\pi \int_0^R \varrho(r) r^2 dr} \mathcal{H}(R - r), \tag{3.17}$$

where $\varrho(r)$ is given in eq. 3.4 and r is the radial component, $\mathcal{H}$ is the Heaviside step function and R is the cutoff of the truncated Gaussian. The truncated Gaussian is, as in regular Ewald summation, added and subtracted from the point charge distribution (see fig. 3.5). This results in a short range potential which is exactly zero at the cutoff, R, for all values of σ. This has implications also in force evaluations as the forces will not diverge at the cutoff (for instance in molecular dynamics or force biased monte carlo). Consequently our method is dependent only on two variables, R and k_{max}, where k_{max} is directly related to the accuracy. σ can then be thought of as a tuning parameter for efficiency in terms of computing time.

Apart from eliminating the σ dependence it is also interesting to see what effect a change in screening function has.

As a continuation of this study it would be interesting to investigate if one could find an optimal choice of σ in terms of time complexity. Also to investigate what happens when σ approaches ∞ as this would result in a screening charge distribution which resembles a square wave function.

3.5 Conducting surfaces

The behaviour of ions close to conducting surfaces is important in many different areas of Science. For instance, the interaction between metallic particles in salt solution. If the particles are large enough, these can be approximated by flat surfaces at short separations. In a electric double layer super capacitor, two conducting electrodes confine an ionic fluid. To be able to simulate such systems, it is important to accurately

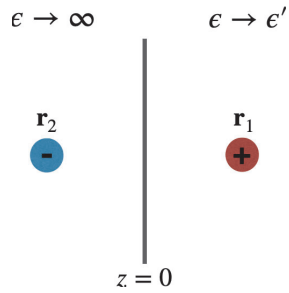

Figure 3.6: Illustration of the image charge ($\mathbf{r}_2$), induced by a charge at $\mathbf{r}_1$. The image charge is reflected across the electrode at $z = 0$ illustrated by a grey line.

model not only the particle-particle interactions, but also the particle-surface interactions. Modelling conducting systems is no easy task due to the complexity of the induced effects in the conductors.

Consider a perfect conductor, inside of which the electrical permittivity $\epsilon(T) = \infty$. It is further infinitely extending in the xy-plane as well as in the region $z < 0$, and is grounded, hence the potential is zero everywhere on its surface. If a charge q is placed a distance d away from the electrode, at say $\mathbf{r}_1 = (x, y, d)$, where the electrical permittivity is distinct from that in the electrode, the charge will induce an opposing surface charge on the conductor. An exact equivalent of this system, which satisfies the same boundary conditions, can be constructed by replacing the electrode with an imagined charge $-q$ at $\mathbf{r}_2 = (x, y, -d)$, see fig. 3.6. The potential from the latter system is

$$\phi(\mathbf{r}) = \frac{1}{4\pi\epsilon(T)'}\left(\frac{q}{|\mathbf{r} - \mathbf{r}_1|} - \frac{q}{|\mathbf{r} - \mathbf{r}_2|}\right). \tag{3.18}$$

This potential satisfies the boundary conditions of the first system, where the potential in the plane $z = 0$ vanishes, as well as when $x, y \to \infty$. Due to reasons that are outside of scope for this thesis, this solution is unique, and hence also the solution for the first system. The solution is however only valid above the surface in the region $z \geq 0$, not in the region $z < 0$, i.e inside the conductor. The second charge is called an *image charge* and the method is called *method of images*[23]. If another electrode is introduced parallel to the first, at say $z = h$ where $h > d$, the image charge in the first electrode will polarize the second electrode, which induces another image charge. This new image charge will in turn again polarize the first electrode. The resulting system is an infinite array of image charges in the z-dimension as if fig. 3.7.

Accounting for image charges in 3D Ewald

In paper II, entitled "Grand canonical simulations of ions between charged conducting surfaces using exact 3D Ewald summations", we present a useful and simple

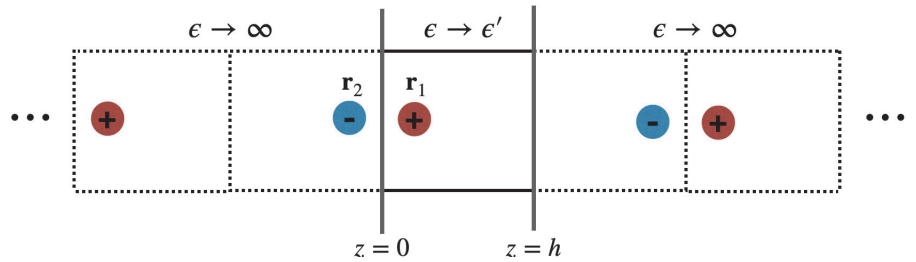

Figure 3.7: Illustration of image charges reflected in two electrodes at $z = 0$ and $z = h$, represented by grey lines. Solid black lines represent edges of the original simulation box and dashed lines represent the image cells. Three dots symbolize a continuation of the image cells.

methodology to simulate charged particles confined by conducting surfaces with constant applied potential. Our methodology exploits the symmetry of the replicas in Ewald summation, and in addition involves a bias potential which enables us to simulate in the grand canonical ensemble at constant electrode potential. The electrostatic interactions between ions and the electrodes are calculated by constructing a unit cell C. C consists of the original simulation cell C_0, centered at origo, with electrodes in the xy-plane at $\pm L/4$. Ions in C_0 with a z-coordinate < 0 are reflected through the left electrode, creating an "image"-cell C_0'. Ions with z-coordinate > 0 are reflected through the right electrode, fig. 3.8. Replicating the unit cell C using regular Ewald summation yields a system with an infinite array of image charges in the z dimension, which is exactly the desired condition for ions confined between conducting surfaces (see section 3.3). In addition, such a system is always electroneutral, as each charge is neutralized by an opposing image charge. However, the total energy of the system would include interactions between the image charges. This is easy to amend for by realizing that the interaction energy of the subcell C_0 with the surrounding cells, is equal to the corresponding energy for subcell C_0'. Thus the energy for C_0 is simply given as half the total energy of C, due to simple symmetry arguments. This construction gives a surface potential (see section 3.7) of zero on both electrodes. Note, however, that the surface potential is not zero compared to a bulk solution.

The individual ion chemical potential for specie i, μ_i, in a bulk electrolyte can be written as

$$\mu_i = \mu - q_i e \psi_{ref} \tag{3.19}$$

where ψ_{ref} is a reference potential. ψ_{ref} is zero for symmetric salts, as in a charge symmetric restricted primitive model for instance, but non-zero for asymmetric salts. Hence, it is a measure of the asymmetry of the electrolyte model.

In our simulations we define an "effective" individual chemical potential using

$$\mu_i' = \mu - q_i e \psi_{bias}. \tag{3.20}$$

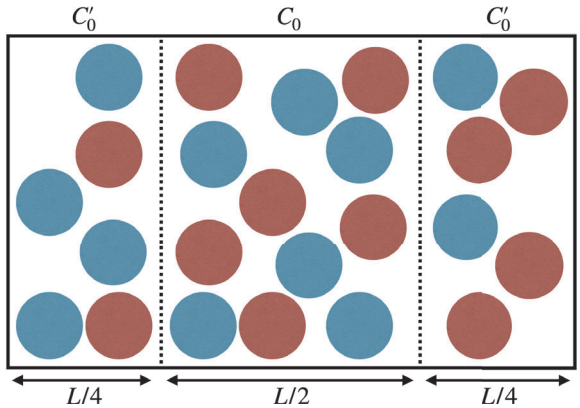

Figure 3.8: Illustration of the unit cell C used in our method.

ψ_{bias} is used to bias either cations or anions to enter the simulation box. The corresponding acceptance criterion in the Metropolis-Hastings algorithm, for an addition of a specie i, (eq. 4.9), becomes

$$a(N_i|N_i+1) = \min\left(1, \frac{V_i}{N_i+1} e^{\beta(\mu_i' - q_i e\psi_{bias})} e^{-\beta(U(\mathbf{r}^{N+1}) - U(\mathbf{r}^N))}\right),$$

where V_i is the total volume accessible to specie i and N_i is the total number of particles of type i.

Using eqs. 3.19 and 3.20 it is possible to write:

$$\mu_i' = \mu_i - q_i e(\underbrace{\psi_{bias} - \psi_{ref}}_{\psi_D}) \tag{3.21}$$

where ψ_D is the Donnan potential. ψ_D is equal to the surface potential of the electrodes relative to the bulk electrolyte and hence can be interpreted as the applied potential. In an unsymmetric salt, where $\psi_{ref} \neq 0$, ψ_{ref} is needed to calculate ψ_D. ψ_{ref} can be measured in a simulation by noting that the potential at the midplane of the simulation box $\phi(z=0) \to -\psi_D$. Provided that the separation between the electrodes is large enough to generate bulk-like conditions at the midplane. So by running a simulation with $\psi_{bias} = 0$, the Donnan potential is simply equal to the reference potential, $\psi_D = \psi_{ref}$ at the midplane.

Our method provides a simple way to simulate both ion behaviour at a single electrode, by using large separation between the electrodes. As well as narrow slits which can be used to mimic a pore in one of the electrodes in a EDLC.

In addition this technique gives us access to the individual chemical potential of the involved species through eq. 3.19.

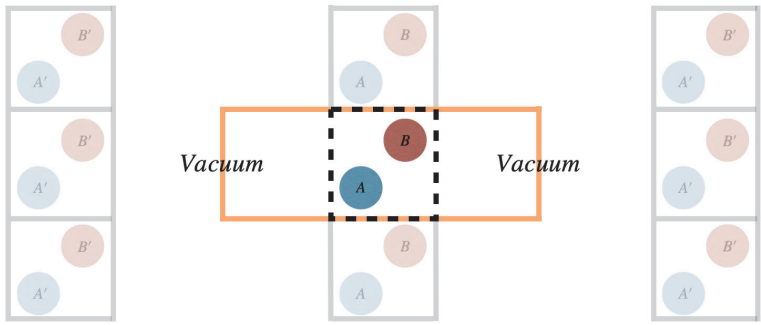

Figure 3.9: Illustration of the Ewald method using vacuum slabs to approximate a slab geometry. The dashed black line indicates the box which confines the particles. The orange box represents the simulation box with the vacuum slits, which is the box replicated in space.

3.6 Non-conducting surfaces

One might think that the treatment of non-conducting surfaces in simulations would be simpler than for conducting surfaces. After all, in such systems there are no image charges to take into account. This is, however, not the case, even though an exact formulation of 2D-Ewald summation exists. Simulation of non-conducting surfaces would be equivalent to only replicating the system in the dimensions which lie parallel to the surfaces, so called quasi-2D. The 2D-Ewald formulation is computationally inefficient, and what one can do instead is use regular 3D Ewald with a modified simulation cell. A slab of vacuum is placed on each side of the simulation box, i.e as in fig 3.9. This yields a system of slab geometry, with non-conducting surfaces. In doing so one has to slightly modify the Ewald energy expression[14] in order to obtain the correct energy. The width of the slabs should be wide enough so that the interaction between the replicates in this dimension in negligible. A slab width of 3-5 times the length of the box in the parallel dimension has been reported to be sufficient[24].

3.7 The surface potential

In these systems an important property is the surface potential. In experiments this potential could represent a voltage difference between the surface and the bulk solution, or another electrode (for instance between anode and cathode). The surface potential is thus the value of the electrical potential at the surface of the electrode, relative to a bulk solution. In experiments it is this potential that is constant, and gives rise to a surface charge.

The potential profile can be calculated by integrating Poisson's equation (eq. 3.1) twice[25]. This is done by using the appropriate boundary conditions. For instance when using conducting surfaces with image charges, the locally measured potential is

zero at both electrodes and hence the boundary conditions are

$$\begin{aligned}\phi(L_1) &= \phi_s = 0 \\ \phi(L_2) &= \phi_s = 0\end{aligned} \tag{3.22}$$

At $z = -\infty$ the electric field vanishes, and therefore we integrate from $-\infty$ to z

$$\frac{d\phi(z)}{dz} = -\int_{-\infty}^{z} \rho(z')dz' + C_1$$

where prime indicates dummy variables. The lower integration limit can be changed to L_1 since there are no charges in the electrode i.e for $z < L_1$, $\rho(z) = 0$. Integrating again yields

$$\phi(z) = -\int_{L_1}^{z}\int_{L_1}^{z'} \rho(z'')dz''dz' + C_1(z - L_1) + C_2 \tag{3.23}$$

Using the boundary conditions in eq. 3.22 we find the constants C_1 and C_2:

$$\begin{aligned}C_1 &= \frac{1}{L_2 - L_1}\int_{L_1}^{L_2}\int_{L_1}^{z} \rho(z')dz'dz \\ C_2 &= 0\end{aligned}$$

Thus the potential profile is given as:

$$\phi(z) = -\int_{L_1}^{z}\int_{L_1}^{z'} \rho(z'')dz''dz' + \frac{z - L_1}{L_2 - L_1}\int_{L_1}^{L_2}\int_{L_1}^{z} \rho(z')dz'dz \tag{3.24}$$

In paper II we use the surface potential to evaluate the correctness of our method. The surface potential is also used when calculating the capacitance, (see Chapter 6).

Chapter 4

Simulations

Molecular simulation is a large field, and as such many different simulation methods have been developed. There are two main branches of molecular simulations. The first contains methods which take quantum effects into account (i.e probability distributions or kinetics of electrons), such methods are aimed as solved the Schrödinger equation, such as Hartree-Fock or DFT. The other branch is classical simulations. In this branch there are no explicit electrons, and the net atomic or molecular charges are often approximated as point charges, as described in the previous chapter.

Markov chain Monte Carlo (MCMC) and Molecular Dynamics (MD) simulations are two commonly used methods in classical molecular modelling. In MD the system is propagated through phase space using Newton's equations of motion. In contrast, MCMC, which is going to be the focus of this chapter, use a more theoretical approach by directly sampling the appropriate probability distribution. The goal of most simulations is to calculate some property, which generally is an average over all microstates in some thermodynamic ensemble. Herein lies the main difficulty in molecular simulation, since the number of microstates often is prohibitively large, a simulation will never be able to visit them all.

Before we dive into the details of MCMC simulations, it is beneficial to look at some differences between MCMC and MD, and when one is preferable over the other. The main difference is how the two methods are propagated. Since MD is propagated using the equations of motion, the result one ends up with, is the particle positions as a function of time. From this, so called *trajectory*, one can calculate any property. Another implication of solving the equations of motion is that the energy is constant, at least in theory. If one also keeps the volume and the number of particles constant, the "inherent" ensemble is thus NVE. If one wishes to simulate in other ensembles

one has to control other parameters, for instance add a thermostat to control the temperature. The perhaps main drawback of MD is that processes that are slow in real life, are also slow in simulations. Such processes could be for instance a binding process or any other process where there is a free energy barrier.

MCMC has the advantage of more freely exploring the free energy landscape, since it relies on direct sampling using the probability distribution of the microstates. This means that one does not care how the system transitions between the microstates, only that these transitions are performed with the correct probability. This means that one can invent moves that propagate the system "unphysically", as long as it does not perturb the final distribution. The downside is then that kinetics are not freely available, since there is no concept of time. There are of course algorithms to aid both MCMC and MD with their downsides, such as dynamic Monte Carlo[26] to approximately capture kinetics in MCMC simulations, or metadynamics[27] to allow MD to more efficiently explore the phase space, and overcome free energy barriers. Now that we have a good grasp on the positives and negatives of MCMC, lets dive into some details.

More formally, a Markov Chain Monte Carlo simulation is a random walk on a weighted and directed graph, which consist of M nodes (microstates), see Fig. 4.1. In this description the "weighted graph" is the Markov chain and Monte Carlo is what drives the "random walk". As we shall see later the random walk is in fact not as random as one would think. Due to the size of phase space a completely random walk would be very inefficient. MCMC instead prioritizes states with high probability and explores *the relevant parts* of phase space little by little using local moves. Although there are differences between continuous Markov chains and discrete Markov chains, only discrete chains will be considered here (generalization to continuous is in many cases straightforward).

4.1 Markov chains

A Markov chain is characterized by a transition matrix (kernel) $\mathbf{T}$ consisting of M^2 elements T_{ij} defining the transition probabilities (weights) of transitioning from state i to state j. Hence row i is the probability of transitioning from state i to any other state. The matrix $\mathbf{T}$ is a stochastic matrix, which implies:

$$\sum_{i}^{N} T_{ij} = 1, \forall j \in \mathcal{S},$$

where $\mathcal{S}$ is, as in the previous chapter the state space, but here each state is represented by an index from 0 to $M-1$. The initial (starting) state is described by a state probability vector $\mathbf{S}^{(0)}$ where each of the M elements is the probability of starting

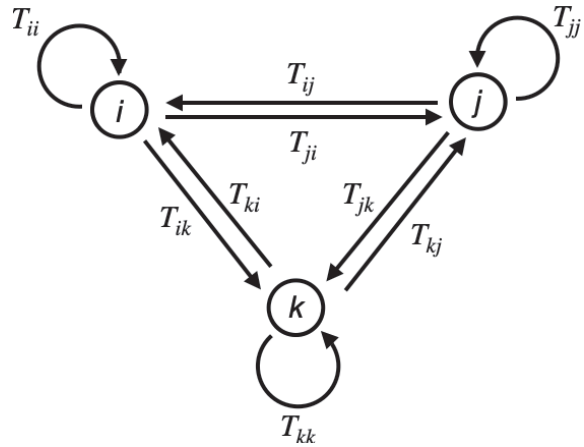

Figure 4.1: A weighted and directed graph with 3 nodes (states) labelled i, j and k. Arrows indicate possible transition paths and T_{ij} is the probability to transition from state i to state j.

in that state. Multiplication by $\mathbf{T}$ yields the state probabilities in the first step in the Markov chain:

$$\mathbf{S}^{(1)} = \mathbf{S}^{(0)}\mathbf{T}.$$

The state probability distribution at the m:th step is therefore:

$$\mathbf{S}^{(m)} = \mathbf{S}^{(m-1)}\mathbf{T},$$

or equivalently:

$$\mathbf{S}^{(m)} = \mathbf{S}^{(0)}\mathbf{T}^{m}.$$

In molecular simulations averages are collected from a given probability distribution, and it is hence required that the state probability vector becomes stationary after a finite number of steps, m, i.e

$$\mathbf{S}^{(t)} = \boldsymbol{\pi}, \forall t \geq m,$$

where π is a stationary distribution. The above equation implies that

$$\boldsymbol{\pi}\mathbf{T} = \boldsymbol{\pi}. \tag{4.1}$$

So to calculate valid averages from some probability distribution, $\boldsymbol{\pi}$ needs to exist (which for a finite Markov chain is always true[28]) and it needs to be independent of the starting state $\mathbf{S}^{(0)}$ i.e it has to be unique. One also needs a way to make sure that $\boldsymbol{\pi}$ is the desired probability distribution that one wants to sample.

Stationary distributions

If a Markov chain is *irreducible*, $\boldsymbol{\pi}$ is unique. In an irreducible Markov chain there is a non-zero probability of going from any state i to any other state j in some number of steps m

$$[p^m]_{ij} > 0, \forall i, j \text{ (for some m)},$$

where $[p^m]_{ij}$ is the probability of being in state i and going to state j in m steps. Thus the chain visits all states if the simulation is run long enough. An irreducible Markov chain is also called an ergodic Markov chain, and guarantees that the stationary distribution is unique[29]. The average state probability distribution is the stationary distribution

$$\lim_{t\to\infty} \frac{1}{t} \sum_{m=1}^{t} \mathbf{S}^{(m)} = \boldsymbol{\pi}, \tag{4.2}$$

$\boldsymbol{\pi}$ is then called a *limiting distribution*. Since $\boldsymbol{\pi}$ is unique, it does not depend on the starting state $\mathbf{S}^{(0)}$, and given enough steps $\boldsymbol{\pi}$ will be reached from any $\mathbf{S}^{(0)}$. Theoretically non-ergodic simulations may seem to not be an issue in molecular simulation. In practice, however, regions in phase space can be separated by large free energy barriers, which practically renders the simulation non-ergodic. It is far from trivial to see if a simulation is ergodic, although there are some techniques to help the system overcome free energy barriers and also to get hints about the ergodic nature of the system[30]. One can, for instance, add large (at least the size of half the box length) occasional displacement moves. Nevertheless, in most molecular systems, ergodicity is an assumed property.

If further the Markov chain is aperiodic, the convergence is absolute, i.e the limit

$$\lim_{m\to\infty} \mathbf{T}^m = \mathbf{T}', \tag{4.3}$$

exists. For an aperiodic state i in the Markov chain there is a non-zero probability for the chain to start in i and revisit i in all future steps i.e

$$[p^m]_{ii} > 0, \ \forall m$$

A simple yet instructive example of a Markov chain which is irreducible but not aperiodic is constructed using the transition matrix:

$$\mathbf{T} = \begin{bmatrix} 0 & 1 \\ 1 & 0 \end{bmatrix}.$$

The chain has two states and starting in either will result in a chain that periodically jumps between the states. Thus the convergence is not absolute as in eq. 4.3, but converges in an average sense as in eq. 4.2.

We now know when the distribution converges and also from eq. 4.1 that the distribution is $\boldsymbol{\pi}$. Intuitively eq. 4.1 means that the probability flow into a state equals the flow out of that state. Hence it is called the *balance equation*. In practice, however, this equation is often of little use and a more stringent condition is often used, called *detailed balance*.

Detailed balance (reversible Markov chains)

By equating each term in the balance condition (eq. 4.1) one arrives at:

$$\pi_i T_{ij} = \pi_j T_{ji}, \forall i, j, \tag{4.4}$$

which is the detailed balance condition. Eq. 4.4 implies reversibility of the Markov chain, i.e the net flow between any two configurations is zero. In the next section we shall see how in practice the detailed balance condition is used to assure that the limiting distribution is our desired distribution.

4.2 Monte Carlo

Due to the enormous amount of microstates in most systems it would not be feasible to simply use the full transition matrix $\mathbf{T}$ in a simulation. Utilizing Monte Carlo however, one can perform a random walk on the Markov chain, and only keep track of the current state. The predominantly used algorithm to perform a random walk on a Markov chain while preserving the correct equilibrium distribution is the Metropolis-Hastings algorithm.

Metropolis-Hastings

In the Metropolis-Hastings algorithm[31,32] the transition matrix is defined as:

$$T_{ij} = q(i|j)\alpha(i|j),$$

where $\alpha(i|j)$ is the probability of accepting a move from state i to state j, and q is the probability of selecting that move. Substituting the above definition of T_{ij} into the detailed balance equation, eq. 4.4,

$$\frac{\alpha(i|j)}{\alpha(j|i)} = \frac{q(j|i)\pi_j}{q(i|j)\pi_i}. \tag{4.5}$$

If $\alpha(i|j)$ is chosen as

$$\alpha(i|j) = \min\left(1, \frac{q(j|i)p_j}{q(i|j)p_i}\right), \tag{4.6}$$

where p is the desired probability distribution, eq. 4.5 is satisfied and $p = \pi$ by construction. Hence the Metropolis-Hastings algorithm provides a way of choosing

the stationary distribution π. The Metropolis-Hastings algorithm is not the only method of choosing a stationary distribution but it is by far the most common in molecular simulation.

4.3 Monte Carlo moves

Many different types of moves can be implemented to propagate the system through a Markov chain. The main goal of Monte Carlo moves is to efficiently (as fast as possible) explore all the degrees of freedom in the ensemble of interest. This is done by first choosing the appropriate probability distribution as the stationary distribution, and then including moves that properly explores all the degrees of freedom of that ensemble. To propagate the system, one is free to choose whichever moves one can think of, however unphysical they may be, as long as the moves obey detailed balance (eq. 4.4), and couple the acceptance criterion of each move with the correct probability distribution. Detailed balance is easily fulfilled for the simplest moves like translation and rotation, since for these moves it is often the case that $q(i|j) = q(j|i)$. The probability of accepting or rejecting such a move, that does not change the number of particles or the volume, is given by the Boltzmann distribution, even if the desired ensemble is not the Canonical. This is valid because the NVT ensemble is a subset of both NPT and μVT. It is straightforward to implement NPT or μVT from an NVT program code, by just adding moves that properly allow the system to explore the new degrees of freedom. A simple algorithm for an MCMC simulation in the canonical ensemble is illustrated below.

1. Choose a random move from a list of possible moves
2. Perform the move (e.g translate or rotate a randomly chosen particle)
3. If the move is accepted, update the current state
4. Collect samples
5. If enough samples are collected, exit the program, otherwise go to step 1

In practice, one more term enters eq. 4.6 namely the probability of selecting "sub-move" type (for instance the addition and deletion moves within a grand canonical simulation). In most cases one does not need to consider this factor but in some circumstances it can be relevant. Say, for instance, that one runs a GC MCMC simulation which includes addition and deletion moves. If the addition move is selected with 30% probability and the deletion move with 10% probability, this has to be taken into account. If the moves are chosen with the same probability, this term cancels.

The canonical ensemble

If we consider rigid particles, with no internal degrees of freedom, in the canonical ensemble, then two moves are sufficient to properly explore the full ensemble: a translation move, and a rotation move. The acceptance probability of a translation or rotation move from state i to state j, is given by substituting the canonical probability density, eq. 2.21, for i and j into the factor $\frac{p_j}{p_i}$, in eq. 4.6. This then yields (since the partition functions cancel):

$$a(i|j) = \min\left(1, e^{-\beta(U_j - U_i)}\right).$$

Due to the detailed balance condition, there are some restrictions on how these moves are allowed to be performed. It is not, for instance, allowed to only rotate in the same direction around the same vector by some angle $< 2\pi$ at each rotation move. Hence, it is common for translation and rotation moves to be constructed such that a reverse move is possible, and chosen with the same probability, i.e $q(j|i) = q(i|j)$. Note that the optimal choice of moves is highly dependent on the nature of the system of interest.

The grand canonical ensemble

In the Grand canonical ensemble, the number of particles is allowed to fluctuate. This introduces one more degree of freedom, as compared to the canonical ensemble. Hence, one needs to include at least two more moves, namely an addition move, and a deletion move. In an addition move, one or more particles are inserted into the simulation box, thus increasing the total number of particles. In a deletion move, particles are removed from the simulation box, decreasing the total number of particles.

Addition move

The acceptance probability of an addition move is given by the same procedure as in the canonical case, in the previous section, by substituting the grand canonical probability density, eq. 2.23, into eq. 4.6. There is one caveat though, that we did not need to concern ourselves with until now. In computer simulations identical particles are *not* indistinguishable[33], since we somehow need to refer to each of them by saving them in some sort of data container (e.g an array). This only has practical implications when changing the number of particles, since in all other cases, any $N!$ terms cancel. Taking this into account and now substituting eq. 2.23 (without the $N!$ term), into

eq. 4.6 we arrive at

$$\frac{p_j}{p_i} = \frac{\frac{1}{\Lambda^{3(N+1)}} e^{\beta(N+1)\mu} e^{-\beta U(\mathbf{r}^{N+1})}}{\frac{1}{\Lambda^{3N}} e^{\beta N \mu} e^{-\beta U(\mathbf{r}^N)}} = \frac{1}{\Lambda^3} e^{\beta\mu} e^{-\beta(U(\mathbf{r}^{N+1}) - U(\mathbf{r}^N))}. \tag{4.7}$$

Often, the factor $\frac{1}{\Lambda^3}$ is absorbed into the chemical potential

$$\mu' = \mu - kT \ln\left(\Lambda^3\right).$$

The resulting μ' is the (relative) chemical potential used in most simulation software.

In contrast to canonical moves, $q(j|i)$ is not generally equal to $q(i|j)$. If the probability to add a particle is equal everywhere inside the simulation box, the probability density of adding at a specific position is $1/V$. Thus $q(i|j) = 1/V$. The probability of reversing the addition (deleting the added particle) is $q(j|i) = \frac{1}{N+1}$. Hence by multiplying eq. 4.7 by $\frac{V}{N+1}$ one ends up with the probability of accepting an addition move:

$$a(N|N+1) = \min\left(1, \frac{V}{N+1} e^{\beta\mu'} e^{-\beta(U(\mathbf{r}^{N+1}) - U(\mathbf{r}^N))}\right).$$

Deletion move

For a deletion move the relations are reversed, a random particle to delete is chosen with probability $1/N$. The probability density of reversing the move (adding back the removed particle) is $\frac{1}{V}$. Hence $q(i|j) = 1/N$ and $q(j|i) = 1/V$. Hence the acceptance probability of deleting a particle is given by:

$$a(N|N-1) = \min\left(1, \frac{N}{V} e^{-\beta\mu'} e^{-\beta\left(U(\mathbf{r}^{N-1}) - U(\mathbf{r}^N)\right)}\right),$$

where again the de Broglie wavelength has been absorbed into the chemical potential.

Single particle GC moves for systems with different species

When performing addition of deletion moves on charged particles, it is often necessary to insert or delete electroneutral groups of molecules, because of the global electroneutrality constraint. In paper II we develop a method, which automatically ensures that the system is electroneutral, irrespective of the number of cations or anions. When using this method one can hence utilize single ion insertions and deletions.

For a general system containing N_{sp} different species, the GC partition function is:

$$Q_{\mu VT} = \prod_{i=1}^{N_{sp}} \left[\sum_{N_i=0}^{\infty} \frac{1}{\Lambda_i^{3N_i}} e^{\beta N_i \mu_i} \int_{\mathcal{S}} e^{-\beta U(\mathbf{r}^{N_i})} d\mathbf{r}^{N_i} \right],$$

where N_i and μ_i are the number of particles and the chemical potential of the i specie. Λ_i is the de Broglie wavelength using the mass of a particle of the i specie. The probability density is:

$$p \propto \prod_{i=1}^{N_{sp}} \frac{1}{\Lambda^{3N_i}} e^{\beta N_i \mu_i} e^{-\beta U(\mathbf{r}^{N_i})}. \tag{4.8}$$

Following the same procedure as in the above case for adding one particle of type i, one arrives at

$$a(N_i|N_i+1) = \min\left(1, \frac{V_i}{N_i+1} e^{\beta\mu_i'} e^{-\beta(U(\mathbf{r}^{N+1})-U(\mathbf{r}^N))}\right). \tag{4.9}$$

where V_i is the volume accessible to specie i.

The isobaric, isothermal ensemble

In the isobaric, isothermal (NPT) ensemble the pressure is kept constant. In MCMC simulations, this is achieved by adding a volume move, which increases or decreases the box volume $V \to V'$. When the move is performed the coordinates of all particles are scaled accordingly, as $\mathbf{r}' = V^{\frac{1}{3}}\mathbf{r}$. Utilizing the NPT probability distribution [6], the acceptance probability is given by

$$a(V|V') = \min\left(1, \left(\frac{V'}{V}\right)^N e^{-\beta p(V'-V)} e^{-\beta(U(\mathbf{r}'^N)-U(\mathbf{r}^N))}\right),$$

and as in the canonical case it is common to choose the volume move such that $q(j|i) = q(i|j)$.

The acceptance ratio of the moves discussed above usually depends on the magnitude of the move (for instance the length of the translation). The optimal choice is not obvious, and there is no generally accepted consensus. A good choice seems to be a set of parameters that leads to an acceptance ratio of about 20-40% [6]. However, in some systems it is not realistic to reach this acceptance, for instance when running grand canonical simulations in dense systems.

4.4 Widom insertion

Widom insertion [34] is a common method used to calculate the chemical potential of the species in a system. Using the definition of the chemical potential in eq. 2.7, the chemical potential can, for large N, be approximated as:

$$\mu \approx F_{N+1} - F_N = -kT \ln\left(\frac{Q_{N+1}}{Q_N}\right),$$

Often one is interested in the excess chemical potential μ' which, using the above equation, can be written as:

$$\mu' = -kT \ln \left\langle e^{-\beta\left(U(\mathbf{r}^{N+1}) - U(\mathbf{r}^{N})\right)} \right\rangle.$$

Thus, in order to measure μ', non-perturbing "ghost" particles are inserted into the simulation box at some interval. The energy difference $U(\mathbf{r}^{N+1}) - U(\mathbf{r}^{N})$ is calculated for each insertion, and the average is then calculated. Non-perturbing in this context means that the inserted particles does not perturb the system in any way, and are removed before the next iteration.

4.5 Correlation

In an MCMC simulation, collected samples are correlated to some extent (depending on how often they are collected). This means that the value of an observable depends on the value at the previous step(s). It can be useful to check how far back this correlation persists, in order to determine a suitable sampling frequency. This can be achieved by plotting the auto-correlation, A, of an observable as a function of the lag time k. The energy autocorrelation, for instance, can be written as:

$$A_U(k) = \int_0^\infty U(t)U(t+k)dt,$$

where t is the time or MCMC step and U is the potential energy.

Chapter 5

Density Functional Theory

Despite the various approximations and optimizations, molecular simulation can be very time consuming, and some properties can be very hard to calculate. A good solution to these problems would be if we had a cheap way to acquire a function for the free energy, since we could derive all other properties from it. There are different methods for acquiring the free energy in MCMC and MD. Many of these methods require a lot of sampling, which is computationally costly for strongly coupled systems, such as ionic solutions with high ionic strength.

The free energy is obviously dependent on the particle positions, or the particle density. Since we know that the free energy is minimized at equilibrium, one can minimize the free energy as a function of the particle density, which then would yield the particle distribution. This is the idea of classical Density Functional Theory (cDFT)[35]. This method is not very unlike its quantum counterpart, quantum DFT where the energy is minimized as a function of the electron density. The goal of cDFT is thus to construct a functional of the form:

$$F\left[n(\mathbf{r})\right] = U\left[n(\mathbf{r})\right] - TS\left[n(\mathbf{r})\right]$$

which then can be minimized with respect to $n(\mathbf{r})$, in order to find the equilibrium density distribution. The following paragraphs is hence devoted to finding expressions for $U\left[n(\mathbf{r})\right]$ and $S\left[n(\mathbf{r})\right]$. Here we will start by introducing the theory on a mean field level, later extending to approximately include spatial correlations. Let us start by finding a function for the entropy, as a function of the particle density. In an ideal gas the particles do not interact with each other, hence $U(\mathbf{r}^N) = 0$. The Helmholtz free energy is then

$$F = -kT \ln\left(\frac{V^N}{N!}\right)$$

If we assume that our system is large, we can use the Stirling approximation, to approximate the factorial in the denominator. The entropy is given as the derivative of the free energy with respect to temperature, we thus get:

$$S = \frac{\partial F}{\partial T} = kN\left(\ln\left(\frac{N}{V}\right) + 1\right)$$

were we can identify N/V as the density n. In a non-homogeneous system the density is a function of $\mathbf{r}$, such that $\int_V n(\mathbf{r})d\mathbf{r} = N$, and the above equation becomes

$$S\left[n(\mathbf{r})\right] = k\int_V n(\mathbf{r})\left(\ln\left(n(\mathbf{r})\right) + 1\right)d\mathbf{r}$$

This form of the entropy does not include any excluded volume effects. These can be incorporated by assuming that each particle occupies a volume V_p. The free available volume is then $V_{free} = V - NV_p$, the entropy then directly follows. We now have a function of the entropy, and what remains is to construct a function for the energy.

Before we begin, we note that in the upcoming sections we will encounter the pair energy as a function of the displacement between two particles, $U(\mathbf{r})$. This energy should be distinguished from the total energy as a function of density, which is denoted $U\left[n(\mathbf{r})\right]$.

A simple approximation for the total energy, is given by the pure mean field energy of a homogeneous particle density n_i, interacting with another particle density n_j. If the interaction potential, $U(\mathbf{r})$, is radially symmetric, the angular parts can be integrated out, which then yields an energy per particle belonging to i, U_p,

$$U_p = 4\pi n_j \frac{1}{2}\int_0^\infty U(r)r^2 dr \tag{5.1}$$

where r is the radial component. An improvement would be to introduce in-homogeneous densities $n(\mathbf{r})$, instead of assuming a uniform density. The mean field energy per particle is then

$$U_p(\mathbf{r}) = \frac{1}{2}\int_V n_j(\mathbf{r}')U(\mathbf{r}-\mathbf{r}')d\mathbf{r}'$$

The total energy, $U\left[n(\mathbf{r})\right]$, is hence:

$$U\left[n(\mathbf{r})\right] = \int_V n_i(\mathbf{r})U_p(\mathbf{r})d\mathbf{r} = \frac{1}{2}\int_V\int_V n_i(\mathbf{r})n_j(\mathbf{r}')U(\mathbf{r}-\mathbf{r}')d\mathbf{r}d\mathbf{r}' \tag{5.2}$$

We now have both components for the free energy functional

$$F[n(\mathbf{r})] = U[n(\mathbf{r})] - TS[n(\mathbf{r})] =$$

$$\frac{1}{2}\int_V \int_V n_i(\mathbf{r}) n_j(\mathbf{r}') U(\mathbf{r}-\mathbf{r}') d\mathbf{r} d\mathbf{r}' + \tag{5.3a}$$

$$\int_V n(\mathbf{r}) U_{ext}(\mathbf{r}) d\mathbf{r} \tag{5.3b}$$

$$kT \int_V n(\mathbf{r}) \ln\left(n(\mathbf{r})-1\right) d\mathbf{r} + \tag{5.3c}$$

where the term in eq. 5.3b takes care of any external potential present in the system.

Here we are mostly interested in systems where an ionic fluid is confined by two charged, and infinitely large planar surfaces. Such a system is in principle one dimensional, if we assume that the particle distributions are uniform in the directions parallel to the surfaces. Using cylindrical coordinates, one can integrate the Coulomb potential in the directions parallel to the surfaces[36], which yields an interaction energy

$$U(z_{ij}) = \frac{1}{4\pi\epsilon(T)} q_i q_j |z_i - z_j| \tag{5.4}$$

inserting this expression into eq. 5.2 yields the total interaction energy

$$U\left[n(z)\right] = -\frac{1}{2}\frac{1}{4\pi\epsilon(T)} \int_0^L \int_0^L n_i(z) n_j(z') q_i q_j |z - z'| dz dz'$$

where L is the distance between the surfaces. In this case $U_{ext}(\mathbf{r})$ is the interaction of an ion with the two charged surfaces. Assuming that the surfaces have charges charges σ_r and σ_l, the interaction energy is given by

$$U_{ext}(z) = -\frac{q}{2\epsilon(T)}(\sigma_l z + \sigma_r(L-z))$$

where if the surface are equally charged, $\sigma_l = \sigma_r = \sigma$ the above equation reduces to

$$U_{ext}(z) = -\frac{q}{2\epsilon(T)}\sigma L \tag{5.5}$$

Combining equations 5.4 and 5.5, the one dimensional free energy now reads

$$F(n(z)) = kT \int_0^L n(z) \ln\left(n(z)-1\right) dz - \tag{5.6a}$$

$$\frac{1}{2}\frac{q_i q_j}{4\pi\epsilon(T)} \int_0^L \int_0^L n_i(z) n_j(z') |z - z'| dz dz' - \tag{5.6b}$$

$$\frac{q}{2\epsilon(T)}\sigma L \int_0^L n(z) dz \tag{5.6c}$$

In our work we are mostly interested in simulating grand canonical systems, which means that the free energy that we want to minimize is the grand potential. The grand potential is related to Helmholtz free energy through a Legendre transform[35]:

$$\Phi\left[n(\mathbf{r})\right] = F\left[n(\mathbf{r})\right] - \mu \int_0^L n(z)dz \tag{5.7}$$

Minimizing the grand potential leads to an expression for the density that can be solved self-consistently:

$$n(z) = \exp\left(\beta\left(\mu - U_{ext} - \int_0^D n(z')U(|z-z'|)dz'\right)\right) \tag{5.8}$$

meaning that first a rough guess is used for the density. Inserting this guess into the equation above yields a better approximation, which then again can be inserted into the expression. In practice inserting the full new density into eq. 5.8 renders the solution unstable. Therefore one uses so called *Picard iterations* where in each iteration the new density inserted into 5.8 is a linear combination of the two previous densities.

Note 5.1. calculating the donnan potential

Consider a system consisting of a salt, confined by two infinitely extending, planar surfaces. The surfaces are equally charged and lie in the (x, y) plane at $z = 0$ and $z = L$. Lets assume that the system initially is not electroneutral but has some net charge A. We thus have that

$$\int_0^L \left(n^+(z) + n^-(z)\right) dz + 2\sigma = A$$

We now wish to calculate a suitable change in the Donna potential, $\Delta\psi_D$ that neutralizes our system. We thus want to calculate a $\Delta\psi_D$ such that

$$\int_0^L \left(e^{q^+\Delta\psi_D} n^+(z) + e^{q^-\Delta\psi_D} n^-(z)\right) dz + 2\sigma = 0$$

where q^+ and q^- are the valencies of the cations and anions respectively. If we now define $e^{\Delta\psi_D} = x$, $\int_0^L n^+(z)dz = N^+$ and likewise for the density of the anions, we get a polynomial expression

$$x^{q^+} N^+ + x^{q^-} N^- + 2\sigma = 0 \tag{5.9}$$

This equation can be solved either analytical, in cases where it is possible, or by a suitable numerical algorithm. Finally the ion densities are updated, as well as the Donnan potential $\psi_D = \Delta\psi_D + \psi_D$

In the case of charged particles, one has to ensure that the system is electroneutral, which can be done through an applied *Donnan potential*, ψ_D. Physically, the Donnan potential represents the potential difference that develops between the system and a bulk solution. The Donnan potential then works to push ions in or out of the system until it is electroneutral. The Donnan potential can therefore be seen as an external potential, which motivates defining, $U_{ext} = U'_{ext} + qe\psi_D$, where U'_{ext} is any other external potential. In practice this amounts to solving for a $\Delta\psi_D$ upon each iteration, which yields an electroneutral system, see note 5.1. To summarize, a schematic algorithm for performing cDFT calculations of an ionic fluid could be

1. Construct the first initial guesses of $n_0^+(z)$ and $n_0^-(z)$
2. Calculate new non-electroneutral densities $n_1^+(z)$ and $n_1^-(z)$ from $n_0^+(z)$ and $n_0^-(z)$, using eq. 5.8
3. Calculate a $\Delta\psi_D$, which gives electroneutral $n_1^+(z)$ and $n_1^-(z)$
4. Use a linear combination to construct the new densities, i.e $n_1^+(z) = \lambda n_1^+(z)' + n_0^+(z)$, where λ typically is around 0.01 to 0.1. The same is done for $n_1^-(z)$.
5. If the difference between $n_1^+(z)$ and $n_0^+(z)$ is smaller than some threshold, the calculation is converged, else set $n_0^+(z) = n_1^+(z)$, $n_0^-(z) = n_1^-(z)$ and go to step 2.

Correlations

The mean field theory overestimates the repulsion between like charged particles, because of the assumption that the particle density is uniform. It is not obvious that this is the case for oppositely charged particles. Since such an interaction includes both an attractive and a repulsive regime. An integral over the attractive and repulsive regimes in such an interaction could then approximately equal zero. Which would in turn mean that the mean field approximation would yield relatively accurate results.

To correct for the overestimation between like charged particles, one could include a suitable approximation of the radial distribution function. One could also simply decrease the interaction of two particles on short distances. This can be done by introducing a so called *Coulomb hole*, in the expression for the energy, $U(r_{ij})$. In paper III we use a Coulomb hole to approximate the correlations between similarly charged particles in the presence of charged surfaces.. The interactions between oppositely charged particles are treated using the mean field approximation. The specific form of the Coulomb hole is given by[37]:

$$U(r_{ij}) = \begin{cases} q_i q_j \frac{1}{r} & \text{if } r > R_c \\ \left(\frac{dU}{dr}\right)_{r=Rc}(r - R_c) + U(r_{ij}) & \text{otherwise} \end{cases} \tag{5.10}$$

This form has the advantage that it is continuous at the cutoff distance. So by for instance approximating the Coulomb potential as a linear function at short range, one would create a Coulomb hole. We used this form of a Coulomb hole in paper III.

Another way to account for correlations would be to approximate the excluded volume of each particle. The simplest form of an excluded volume would be the Heaviside step function. This would correspond to a depleted region around each particle and would be equivalent to hard sphere particles. The Heaviside step function is defined as

$$\Theta(r) = \begin{cases} 0 \text{ if } r < 0 \\ 1 \text{ otherwise} \end{cases}$$

In practice this is done by modifying eq. 5.3a

$$\frac{1}{2}\int_V \int_V n(\mathbf{r})\Theta\left(|\mathbf{r}-\mathbf{r}'| - \frac{1}{2}d\right) n(\mathbf{r}')U(|\mathbf{r}-\mathbf{r}'|)d\mathbf{r}d\mathbf{r}' \tag{5.11}$$

where d is typically chosen to be the diameter of a particle.

Chapter 6

Behaviours of Ions in Slab Systems

Charged particles are ubiquitous in our everyday life. They exist in the appliances and electronics we use and the food that we eat, not to mention in the majority of the waters. Charged particles are also vital in biological systems, for instance charged proteins in our cells or salts in our blood. Therefore it is of fundamental importance that we understand how charged particles behave in different environments. Here we mainly focus on how charged particles interact with charged surfaces. This approach has the benefit of representing two different types of systems. The first is simply ions interacting with a charged surface. The second is ions interacting with a charged macroparticle. Consider a small ion interacting with a much larger macroparticle. In the eyes of the ion, the macroparticle will behave like a flat surface.

The ions close to a charged surface will form a so-called electrical double layer (EDL).

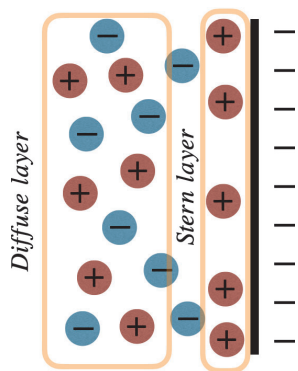

Figure 6.1: Illustration of a negatively charged surface (thick black vertical line), along with the Stern and diffuse layers (orange boxes) formed by the ions.

The ions with an opposite charge to that of the surface (the counter-ions) attract to the surface, and the innermost layer of counter-ions is called the *Stern layer*. These ions are normally only laterally mobile. The counter-ions which has adsorbed on the surface in turn attracts co-ions (i.e ions with a charge of the same sign as the surface charge), which together with other counter-ions form an outer layer, called the *diffuse layer*. This EDL model is depicted in fig. 6.1. The structure and formation of the EDL is interesting from a number of perspectives. It has implications for how charged macroparticles interact in a solution containing ions and is also important in electric double layer capacitor systems.

Many different methods have been developed to model EDLs and the interaction between charged surfaces in an ionic solution. The simplest is perhaps the Poisson-Boltzmann theory (PB)[38]. In PB theory, the charge density of the Poisson equation, 3.1, is assumed to follow the Boltzmann probability distribution, derived in an earlier chapter. In one dimension this amounts to

$$\rho(z) = c_0 e^{-\beta q e \psi(z)} \tag{6.1}$$

where $qe\psi(z)$ is the potential energy of an ion placed at z in the potential field $\psi(z)$, and c_0 is the bulk density. $\psi(z)$ can be composed of an external potential, as well as the interaction between particles. In PB theory, this inter-particle interaction is taken into account in a mean field manner, meaning that a given particle interacts with the average distribution of the other particles. This yields a particle density

$$\rho(z) = c_0 \exp\left(-\beta(U_{ext}(z) + \int n(z')U(z-z')dz')\right) \tag{6.2}$$

As a side note this density is equal to the density of the cDFT formulation, neglecting correlations. Typically this method works quite well for describing ions in the diffuse layer in systems where the ion valency is not too high. Often the Stern layer is much more dense than the diffuse layer, and therefore ion correlations become more important.

Another popular method to calculate the interaction between surfaces or macromolecules in ionic solutions is DLVO[39]. DLVO considers two main contributions to the interactions between the surfaces. An attractive van der Waals component acting on short range, and an electrostatic component which models the repulsion generated when two electrical double layers overlap. The electrostatic term is in the form of a screened Coulomb potential. Hence direct ion-ion correlations in the intervening solution are ignored.

As we will see in the upcoming sections, including ion correlations changes the behaviour of the system. At strong electrostatic coupling, it is no longer a feasible approximation to ignore ion correlations.

6.1 Modelling ions in computer simulations

Charged particles come in many different shapes and forms, from small single atom ionic species, to large macromolecules. In our research, we have used crude models, which capture the essentials of what an ion is. We approximate the ions as both soft and hard spheres (papers III, IV and V respectively), containing a single point charge. In doing so we thus reduce the number of internal degrees of freedom of the particles. This method of reducing the internal degrees of freedom is called coarse graining. Our particle models might seem as a gross simplification, but it turns out that such a simple model is able to capture some of the more complex behaviour of real ions.

There are, however, limits to where such models are applicable and obviously, such an ion model will not behave exactly as a real ion. There are two main reasons for these simplifications. The first, and obvious one, is computational. Since we are removing the internal degrees of freedom of the ions, we are reducing the complexity of the problem. Hence, our simulations take less time to perform. The second reason, is that there is scientific value in reducing the number of parameters. If we only have a few parameters, it is much easier to elucidate the main mechanisms behind complex behaviour.

Our ion models are all variants of the Restricted Primitive Model (RPM). In the RPM, the anion and cation are spherical particles with central point charges. Both ions have a common radius, as well as the same valency. One problem with the RPM model is the symmetry, both internally and between the ions. With our models we try to capture some of the asymmetric elements of real ions, to enable more complex behaviour.

6.2 Ion correlations

Introducing correlations between ions enables more complex behaviour, especially in slit geometries. One interesting phenomena is correlation induced attraction of equally charged surfaces at short range [40,41]. This attraction only appears if correlations between counter-ions are taken into account, and the electrostatic coupling is strong enough. It is hence dependent on the surface charge and ionic strength. In such systems, PB predicts a strong repulsion in these circumstances. In fig. 6.2 the free energy of interaction between two equally charged surfaces if plotted as a function of separation h. The free energies have been calculated using cDFT with and without correlations between counter-ions, as explained in an earlier chapter. From this figure it is clear that the short range attraction only appears as correlation between counter ions are present.

Another correlation induced phenomenon is overcharging [42]. Overcharging, or charge

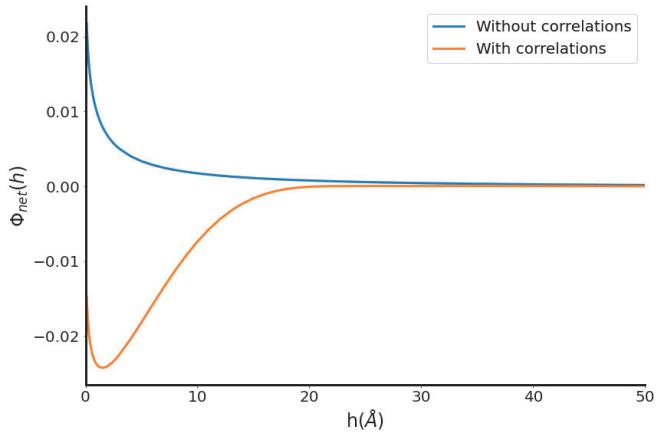

Figure 6.2: Free energy of interaction between two equally charged surfaces, plotted against the separation distance h. The salt concentration is in both cases 1mM while the surface charge is 0.01e/Å on both surfaces.

reversal as it is also called, is where the counter-ions overcompensate the surface charge. Thereby effectively reversing the sign of the potential some distance away from the surface. This effect is of course dependent on the electrostatic coupling and ionic strength. Overcharging in turn generates secondary effects such as long range attraction or repulsion between like-charged, or neutral, surfaces. These effects are hence very important for the stability of colloidal dispersions. Papers III and IV is a two part study of overcharging and related effects.

In paper III, "Overcharging and Free Energy Barriers for Equally Charged Surfaces Immersed in Salt Solutions", we study this overcharging behaviour using a combination of cDFT and MC. Specifically our system consists of multivalent counter-ions and monovalent co-ions, confined by charged, non-conducting surfaces. In previous studies, significant attention has been devoted to the short range correlation attraction between charged surfaces. In this paper we instead focus on the interactions at long range. In particular we show that our investigated systems display overcharging, and that it is due to the correlations between the counter-ions.

We investigate the concentration dependence of this overcharging, and find that at high salt concentration the surfaces overcharge, effectively reversing the sign of the inherent surface charge. At these conditions there is a significant free energy barrier between the surfaces. At low salt concentration on the other hand the surfaces are undercharged, again resulting in a free energy barrier. At intermediate concentrations we find a critical concentration where the surfaces are perfectly neutralized. In this regime the free energy barrier disappears, which would destabilize a colloid suspension. As such, in this paper, we demonstrate a clear relationship between the apparent

surface charge and the interaction free energy between two charged non-conducting surfaces.

This study is continued in paper IV, "Interactions between conducting surfaces in salt solutions", where we investigate a similar system but with conducting surfaces. Here we use the method developed in paper II, to study overcharging and surface neutralization when conducting surfaces are present. Due to the complexity of handling conducting surfaces, such systems have not been studied as much as non-conducting surfaces. In this study again find a non-monotonic dependence of the surface charge on the salt concentration. However, in contrast to non-conducting surfaces, we find a large repulsion between non-charged surfaces. This repulsion is generated by the adsorption of multivalent counter-ions on the surfaces. In addition, we show a clear relationship between the apparent surface charge and the interaction free energy barriers between the surfaces. We also explicitly show the existence of a critical concentration where the surfaces are neutralized, above which the surface have a charge and below which the charge is inversed. We also show that that the particle surface interaction can be succesfully modelled by a simple interaction potential, which drastically decreases the computational complexity. Our simple interaction potential is linear and has the form:

$$\beta U = \begin{cases} -A_w q^2 \left(1 - \frac{z-d/2}{d}\right), \text{ if } \frac{d}{2} \leq z \leq \frac{3d}{2} \\ 0, \text{ otherwise} \end{cases} \tag{6.3}$$

6.3 Image charge effects

It turns out that when conducting surfaces are present, even more behaviours emerge. In particular one can find an anomalous charging regime, where the magnitude of the overcharging is increasing with *decreasing* surface charge density. In this section we will simulate a system which displays this behaviour, using the method from paper II. Our system consists a simple $2:1$ salt, where the cation and anion share a common radius of 2Å. The ions are confined by two infinitely conducting electrodes, placed at $z = -100$Åand $z = 100$Å. For comparison, the same setup but with non-conducting electrodes is also simulated. There is one important difference between these two simulations. While the simulations with non-conducting surfaces are performed in a constant charge density ensemble, here called σ-control, the simulations with conducting surfaces are performed in an constant potential ensemble, ψ-control. Consequently, in the following section, the reported surface charge densities, σ, in the case of conducting surfaces are averages, while when using non-conducting surfaces σ is an input parameter. In both cases, the chemical potential is adjusted so that the bulk density is about 100mM.

In fig. 6.3 we have plotted the apparent surface charge against the z-coordinate of

the system with non-conducting surfaces. Here it is clear that the strength of the overcharge (the maximum of the apparent surface charge) is increased as the surface charge is increased.

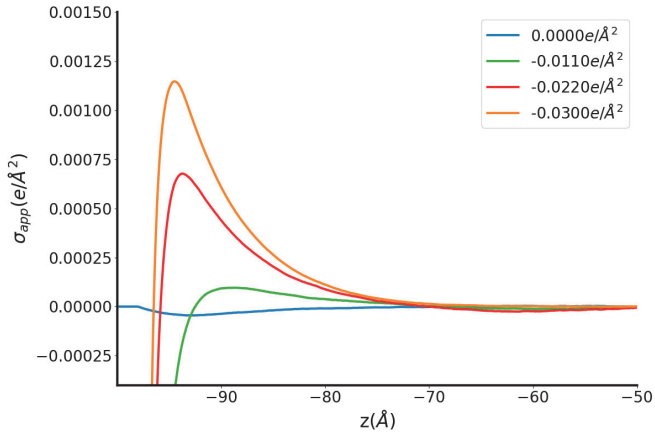

Figure 6.3: Apparent surface charge for a $2:1$ salt simulated using σ-control at different surface charges.

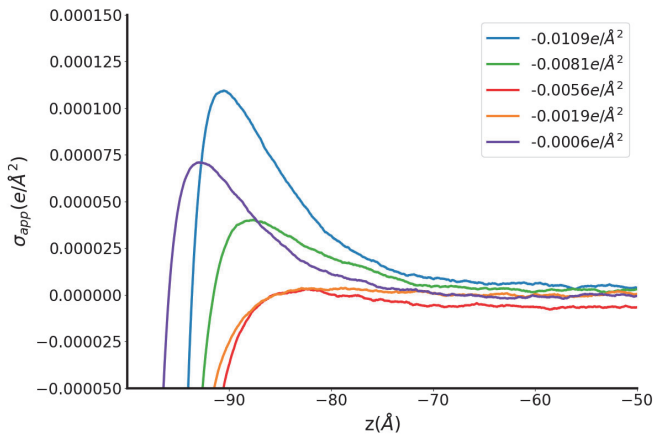

Figure 6.4: Apparent surface charge for a $2:1$ salt simulated using ψ-control, at different applied bias potentials.

When the surfaces are made conducting, the charges are further attracted towards the discontinuity by their image charge. The increased attraction results in a considerable increase in the overcharge, as expected. A not so expected behaviour is that of the overcharge as the surface charge is varied. In fig. 6.4 the results for a 2:1 salt near conducting surfaces is shown. Here one can observe that there is a regime where the strength of the overcharge increases as the surface charge becomes more positive, the opposite of what one would expect. One might be tempted to attribute this behaviour

to saturation of counter-ions at the surfaces. This is however not the case as evident by fig. 6.5. In this figure, a snapshot from a simulation of the ions close to one of the surfaces is shown, and it is clear that the surface is not saturated. Further evidence for this is shown in fig. 6.6, where the ion density profiles are plotted. From this figure it is clear that the counter-ion concentration at the surface increases, as the surface charge increases.

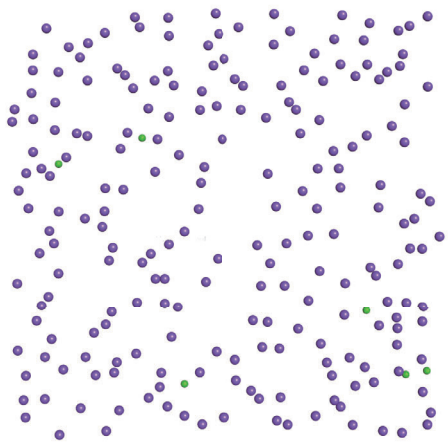

Figure 6.5: Snapshots of ions with a z-coordinate $z < 5$Å. Purple spheres are cations and green spheres are anions

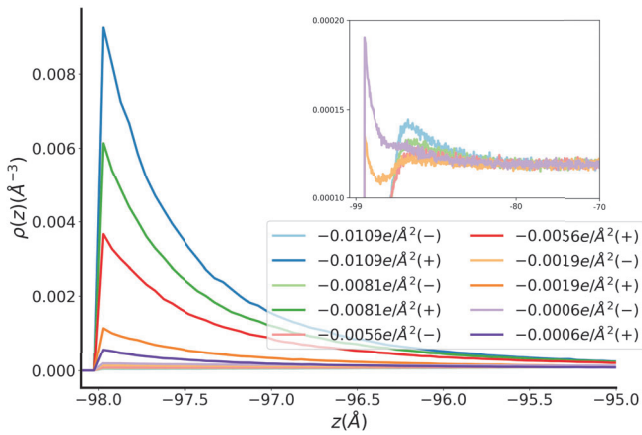

Figure 6.6: Ion densities for the 2:1 salt. A magnified version of the anion density profile is shown in the insets.

Two clear peaks in the density of the co-ions can be seen in fig. 6.6. The magnitude of the inner peak is increased as the surface charge is increased, while the outer peak displays the opposite trend. From this we can identify two different charging regimes.

At a strong negative surface charge, $-0.0109e/\text{Å}$ to $-0.0056e/\text{Å}$, the divalent cations are strongly attracted to the surface due to the inherent (negative) surface charge and also due to the image charges. This leads to an overcompensation of the surface charge. Thus attracting co-ions which reside in the second particle layer resulting in a single peak of the co-ion density, which can be seen in the inset of fig. 6.6. This peak increases in magnitude as σ is made more negative, to compensate for the increase in counter-ions in the Stern layer. In this regime the overcharging increases when $|\sigma|$ increases (becomes more negative). As the surface charge is increased (made more positive), the co-ions will attract closer to the surface as the attraction to the image charge overcomes the repulsion from the surface charge and loss of entropy. This results in the formation of a second peak in the density of the co-ions, which lie in the Stern layer. This peak increases with increasing (more positive) surface charge. Hence the innermost layer now consists of both counter-ions and co-ions. As the surface charge continues to increase, the concentration of co-ions increases in the Stern-layer. In this regime the overcharging increases with *decreasing* $|\sigma|$.

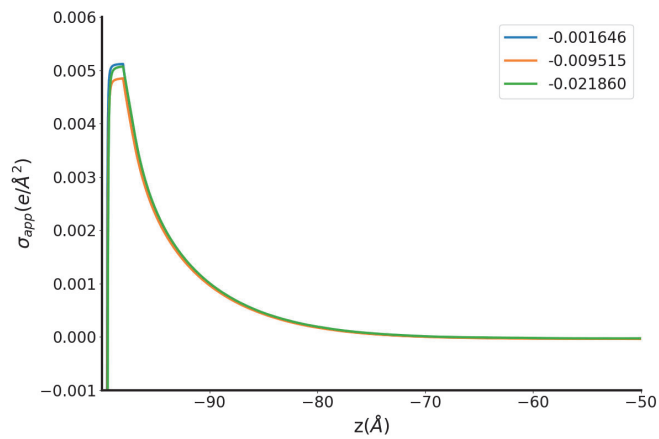

Figure 6.7: Apparent surface charge for a $2:1$ salt simulated using ψ-control, at different applied bias potentials. Cation radius is set to $r = 0.5$Å

This interesting behaviour persists if the radius of the cations is made smaller. In figs. 6.7 and 6.8 we have plotted results for an RPM-like salt, where the radius of the cation is decreased. In fig. 6.7 the radius is set to 0.5Å while in 6.8 it is 1Å. In both cases the radius of the anions is 2Å, as in the previous case. This ion model displays the same trends, and approximately the same magnitude of the overcharge.

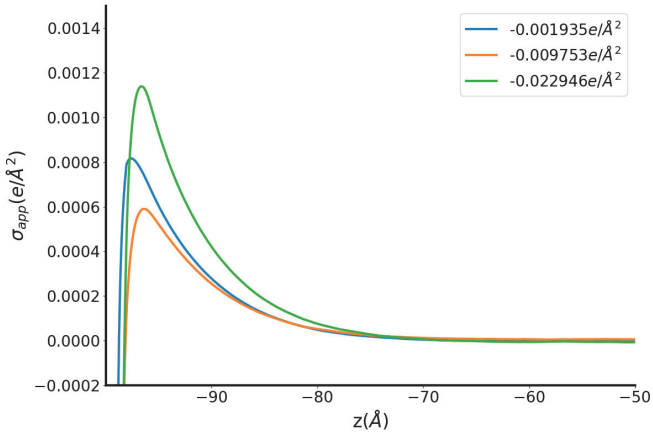

Figure 6.8: Apparent surface charge for a $2:1$ salt simulated using ψ-control, at different applied bias potentials. Cation radius is set to $r = 1$Å

6.4 Capacitors

Capacitors are one of the fundamental building blocks in electronic circuits, and are used in a variety of different contexts, such as alternating current to direct current conversion, timing circuits and signal filtering. A capacitor is similar to a battery in that it stores electrical energy. Typically a capacitor consists of a dielectric material sandwiched between two electrodes. If a voltage (electric potential difference) is applied across the capacitor, the dipoles in the dielectric aligns to oppose the resulting electric field, which is the storage mechanism in a conventional capacitor.

In contrast to a battery a capacitor has much lower energy density but higher power density, meaning they can not store as much energy, but can charge and discharge much faster. This property makes capacitors ideal in situations where a quick burst of energy is needed as for instance in camera flashes and braking systems. In addition there are no chemical reactions in the charging and discharging process of a capacitor, which increases the maximum number of recharge cycles to way beyond that of batteries. The integral capacitance, c, is a measure of the storage capacity of a capacitor. The integral capacitance is

$$c = \frac{\sigma}{\phi_s},$$

where σ is the surface charge on the electrodes resulting from a surface potential (voltage) ϕ_s. In an ideal, so called parallel-plate capacitor, the capacitance is directly proportional to the surface area of the electrodes and inversely proportional to the distance between them:

$$c = \frac{\epsilon_0 \epsilon_r A}{d}, \tag{6.4}$$

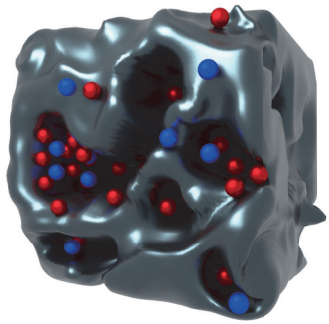

Figure 6.9: Crude sketch of a porous electrode. Blue and red spheres represent anions and cations respectively.

where A is the area of the electrode and d is the distance between the electrodes.

In electric double layer super capacitors (EDLCs) the dielectric is replaced by an electrolyte, where room temperature ionic liquids is a promising choice[43,44]. When a potential is applied across an EDLC, cations accumulate on the anode and anions on the cathode. EDLCs store energy in the formed double layers at the electrode-ion interface. The charges in the electrolyte are able to approach very closely to the electrode surface which greatly increase the capacitance (see eq. 6.4). Also, since the capacitance is proportional to the surface area of the electrodes, EDLCs are often constructed using porous electrodes, see fig. 6.9.

An EDLC pore (inside a porous electrode) can in simulations be approximated by two flat surfaces confining an ionic liquid. The electrostatic interactions between ions and electrodes, in such a system, can be calculated using methods explained earlier (see section 3.3). A direct summation of all the ions and image charges is, however, very inefficient. There has been a lot of research on how to efficiently calculate the image charge interactions[45,46,47,48,49].

In comparison with the integral capacitance, the differential capacitance, c_D, is more informative about the charging process. The differential capacitance is defined as:

$$c_D(\phi_s) = \frac{d\sigma(\phi_s)}{d\phi_s}, \tag{6.5}$$

where σ is the surface charge density. The differential capacitance is an important property since the surface charge in many EDLC systems is not a linear function of the applied voltage[50]. To calculate the differential capacitance in a simulation setting, several simulations are performed of the same system but at different applied potential. In each simulation the average surface charge is calculated and $c_D(\phi_s)$ can then be plotted.

In paper V, "Simulations of phase transitions and capacitance, of simple ionic fluids

in porous electrodes.", we study a simple RPM salt confined between conducting and non-conducting surfaces. With such a setup, we try to mimic a pore in a porous electrode, in an EDLC. Our aim is to systematically investigate under which conditions our system displays a negative capacitance, and the general behaviour at near-critical conditions.

Using Grand Canonical simulations, to properly account for the equilibrium between our system and a bulk solution, we study a dilute ionic fluid, which may undergo capillary condensation, if the surface charge density is high enough. We simulate this system in both a constant potential and a constant surface charge density ensemble. In the constant charge simulations we use explicit charges on the surfaces. The surface charges are placed in a 2D lattice on each surface at the start of the simulation. They are immobile and does not move during the simulation. We replicate the system in space using Ewald summation with vacuum slabs. The constant potential simulations are performed in the same manner, but instead of ion pairs, individual ions are inserted each GC step. This way the surface charge fluctuates while the surface charge stays constant.

We find that in a constant potential ensemble, the capacitance is positive for all investigated cases. At some critical applied potential the surface charge density displays a sudden jump, coinciding with the phase transition to the denser phase. Using non-conducting surface we further find that such a system may display a hysteresis, which means that at a given applied potential, the system may be in either two states. Hence when using non-conducting surfaces, the meta stable states seem to be stabilized, as compared to the case of conducting surfaces.

In a constant surface charge density ensemble, we find regions where the potential decreases with increasing surface charge, indicating a negative capacitance.

We also investigate how these behaviours are affected by pore width. By running simulations at different separations, we find that both the jump and the negative capacitance is lost, if the pore is made narrow. At larger pore widths, the constant potential simulations display a first order phase transition, causing a sudden jump in the surface charge density. For the constant surface charge density simulaitons we observe a metastable region between the two states.

References

[1] Alexey V. Onufriev and Saeed Izadi. Water models for biomolecular simulations. *WIREs Computational Molecular Science*, 8(2):e1347, 2018. doi: 10.1002/wcms.1347.

[2] David van der Spoel, Paul J. van Maaren, and Herman J. C. Berendsen. A systematic study of water models for molecular simulation: Derivation of water models optimized for use with a reaction field. *The Journal of Chemical Physics*, 108(24):10220–10230, 1998. doi: 10.1063/1.476482.

[3] Péter T. Kiss and András Baranyai. Sources of the deficiencies in the popular spc/e and tip3p models of water. *The Journal of Chemical Physics*, 134(5):054106, 2011. doi: 10.1063/1.3548869.

[4] Feng Chen and Paul E. Smith. Simulated surface tensions of common water models. *The Journal of Chemical Physics*, 126(22):221101, 2007. doi: 10.1063/1.2745718.

[5] Otto Redlich. Intensive and extensive properties. *Journal of Chemical Education*, 47(2):154, 1970.

[6] Daan Frenkel and Berend Smit. *Understanding molecular simulation : from algorithms to applications. 2nd ed*, volume 50. 01 1996. doi: 10.1063/1.881812.

[7] Lev Davidovich Landau and Evgenii Mikhailovich Lifshitz. *Course of theoretical physics*. Elsevier, 2013.

[8] Jan T. Knuiman, Peter A. Barneveld, and Nicolaas A. M. Besseling. On the relation between the fundamental equation of thermodynamics and the energy balance equation in the context of closed and open systems. *Journal of Chemical Education*, 89(8):968–972, 2012. doi: 10.1021/ed200405k.

[9] Kenneth Franklin Riley, Michael Paul Hobson, and Stephen John Bence. Mathematical methods for physics and engineering, 1999.

[10] Thomas M. Nymand and Per Linse. Ewald summation and reaction field methods for potentials with atomic charges, dipoles, and polarizabilities. *The Journal of Chemical Physics*, 112(14):6152–6160, 2000. doi: 10.1063/1.481216.

[11] P. P. Ewald. Die berechnung optischer und elektrostatischer gitterpotentiale. *Annalen der Physik*, 369(3):253–287, 1921. doi: 10.1002/andp.19213690304.

[12] S. W. de Leeuw, J. W. Perram, E. R. Smith, and John Shipley Rowlinson. Simulation of electrostatic systems in periodic boundary conditions. i. lattice sums and dielectric constants. *Proc. R. Soc. A*, 373(1752):27–56, 1980. doi: 10.1098/rspa.1980.0135.

[13] Zhonghan Hu. Infinite boundary terms of ewald sums and pairwise interactions for electrostatics in bulk and at interfaces. *Journal of Chemical Theory and Computation*, 10(12):5254–5264, 2014. doi: 10.1021/ct500704m. PMID: 26583209.

[14] In-Chul Yeh and Max L Berkowitz. Ewald summation for systems with slab geometry. *The Journal of chemical physics*, 111(7):3155–3162, 1999.

[15] Jochen S. Hub, Bert L. de Groot, Helmut Grubmüller, and Gerrit Groenhof. Quantifying artifacts in ewald simulations of inhomogeneous systems with a net charge. *Journal of Chemical Theory and Computation*, 10(1):381–390, 2014. doi: 10.1021/ct400626b. PMID: 26579917.

[16] Brad A. Wells and Alan L. Chaffee. Ewald summation for molecular simulations. *Journal of Chemical Theory and Computation*, 11(8):3684–3695, 2015. doi: 10.1021/acs.jctc.5b00093. PMID: 26574452.

[17] Tom Darden, Darrin York, and Lee Pedersen. Particle mesh ewald: An nlog(n) method for ewald sums in large systems. *The Journal of Chemical Physics*, 98(12):10089–10092, 1993. doi: 10.1063/1.464397.

[18] Ulrich Essmann, Lalith Perera, Max L. Berkowitz, Tom Darden, Hsing Lee, and Lee G. Pedersen. A smooth particle mesh ewald method. *The Journal of Chemical Physics*, 103(19):8577–8593, 1995. doi: 10.1063/1.470117.

[19] Henk Bekker, HJC Berendsen, EJ Dijkstra, S Achterop, R Vondrumen, David VANDERSPOEL, A Sijbers, H Keegstra, and MKR Renardus. Gromacs-a parallel computer for molecular-dynamics simulations. In *4th International Conference on Computational Physics (PC 92)*, pages 252–256. World Scientific Publishing, 1993.

[20] Romelia Salomon-Ferrer, David A Case, and Ross C Walker. An overview of the amber biomolecular simulation package. *Wiley Interdisciplinary Reviews: Computational Molecular Science*, 3(2):198–210, 2013.

[21] Aidan P Thompson, H Metin Aktulga, Richard Berger, Dan S Bolintineanu, W Michael Brown, Paul S Crozier, Pieter J in't Veld, Axel Kohlmeyer, Stan G Moore, Trung Dac Nguyen, et al. Lammps-a flexible simulation tool for particle-based materials modeling at the atomic, meso, and continuum scales. *Computer Physics Communications*, 271:108171, 2022.

[22] Jiri Kolafa and John W Perram. Cutoff errors in the ewald summation formulae for point charge systems. *Molecular Simulation*, 9(5):351–368, 1992.

[23] Marius M. Hatlo and Leo Lue. The role of image charges in the interactions between colloidal particles. *Soft Matter*, 4:1582–1596, 2008. doi: 10.1039/B803783C.

[24] Paul S Crozier, Richard L Rowley, Eckhard Spohr, and Douglas Henderson. Comparison of charged sheets and corrected 3d ewald calculations of long-range forces in slab geometry electrolyte systems with solvent molecules. *The Journal of Chemical Physics*, 112(21):9253–9257, 2000.

[25] Dezső Boda and Dirk Gillespie. Calculating the electrostatic potential profiles of double layers from simulation ion density profiles. *Hungarian Journal of Industrial Chemistry*, 41:123–130, 2013.

[26] Kristen A Fichthorn and W Hh Weinberg. Theoretical foundations of dynamical monte carlo simulations. *The Journal of chemical physics*, 95(2):1090–1096, 1991.

[27] Alessandro Laio and Michele Parrinello. Escaping free-energy minima. *Proceedings of the National Academy of Sciences*, 99(20):12562–12566, 2002.

[28] A Furman. What is a stationary measure? *Notices of the AMS*, 58:1276–1277, 2011.

[29] Charles M. Grinstead and J. Laurie Snell. *Introduction to Probability*. AMS, 2003.

[30] J. P. Neirotti, David L. Freeman, and J. D. Doll. Approach to ergodicity in monte carlo simulations. *Phys. Rev. E*, 62:7445–7461, 2000. doi: 10.1103/PhysRevE.62.7445.

[31] Nicholas Metropolis, Arianna W. Rosenbluth, Marshall N. Rosenbluth, Augusta H. Teller, and Edward Teller. Equation of state calculations by fast computing machines. *The Journal of Chemical Physics*, 21(6):1087–1092, 1953. doi: 10.1063/1.1699114.

[32] W. K. Hastings. Monte Carlo sampling methods using Markov chains and their applications. *Biometrika*, 57(1):97–109, 04 1970. ISSN 0006-3444. doi: 10.1093/biomet/57.1.97.

[33] Robert H Swendsen. Statistical mechanics of classical systems with distinguishable particles. *Journal of statistical physics*, 107(5):1143–1166, 2002.

[34] B. Widom. Some topics in the theory of fluids. *The Journal of Chemical Physics*, 39(11):2808–2812, 1963. doi: 10.1063/1.1734110.

[35] Sture Nordholm, Jan Forsman, Cliff Woodward, Ben Freasier, Zareen Abbas, and Robert Penfold. *Generalized Van Der Waals Theory of Molecular Fluids in Bulk and at Surfaces*. Elsevier, 2018.

[36] Sture Nordholm, Jan Forsman, Cliff Woodward, Ben Freasier, Zareen Abbas, and Robert Penfold. *Generalized Van Der Waals Theory of Molecular Fluids in Bulk and at Surfaces*. Elsevier, 2018.

[37] Jan Forsman. A simple correlation-corrected poisson- boltzmann theory. *The Journal of Physical Chemistry B*, 108(26):9236–9245, 2004.

[38] Terrell L Hill. *An introduction to statistical thermodynamics*. Courier Corporation, 1986.

[39] Evert Johannes Willem Verwey and J Th G Overbeek. Theory of the stability of lyophobic colloids. *Journal of Colloid Science*, 10(2):224–225, 1955.

[40] Roland Kjellander and Stjepan Marčelja. Interaction of charged surfaces in electrolyte solutions. *Chemical physics letters*, 127(4):402–407, 1986.

[41] JP Valleau, R Ivkov, and GM Torrie. Colloid stability: The forces between charged surfaces in an electrolyte. *The Journal of chemical physics*, 95(1):520–532, 1991.

[42] Christophe Labbez, Bo Jonsson, Michal Skarba, and Michal Borkovec. Ion-ion correlation and charge reversal at titrating solid interfaces. *Langmuir*, 25(13): 7209–7213, 2009.

[43] Cheng Zhong, Yida Deng, Wenbin Hu, Jinli Qiao, Lei Zhang, and Jiujun Zhang. A review of electrolyte materials and compositions for electrochemical supercapacitors. *Chem. Soc. Rev.*, 44:7484–7539, 2015. doi: 10.1039/C5CS00303B.

[44] Ander González, Eider Goikolea, Jon Andoni Barrena, and Roman Mysyk. Review on supercapacitors: Technologies and materials. *Renewable and Sustainable Energy Reviews*, 58:1189 – 1206, 2016. ISSN 1364-0321. doi: https://doi.org/10.1016/j.rser.2015.12.249.

[45] Alexandre P. dos Santos, Matheus Girotto, and Yan Levin. Simulations of coulomb systems confined by polarizable surfaces using periodic green functions. *The Journal of Chemical Physics*, 147(18):184105, 2017. doi: 10.1063/1.4997420.

[46] Sandeep Tyagi, Axel Arnold, and Christian Holm. Icmmm2d: An accurate method to include planar dielectric interfaces via image charge summation. *The Journal of Chemical Physics*, 127(15):154723, 2007. doi: 10.1063/1.2790428.

[47] Sandeep Tyagi, Axel Arnold, and Christian Holm. Electrostatic layer correction with image charges: A linear scaling method to treat slab 2d+h systems with dielectric interfaces. *The Journal of Chemical Physics*, 129(20):204102, 2008. doi: 10.1063/1.3021064.

[48] R. Kjellander and S. Marcelja. Electrical double layer interactions with image charges. *Journal of Physical Chemistry*, 82(12), 1984.

[49] Stewart K. Reed, Oliver J. Lanning, and Paul A. Madden. Electrochemical interface between an ionic liquid and a model metallic electrode. *The Journal of Chemical Physics*, 126(8):084704, 2007. doi: 10.1063/1.2464084.

[50] Celine Merlet, Benjamin Rotenberg, Paul A. Madden, Pierre-Louis Taberna, Patrice Simon, Yury Gogotsi, and Mathieu Salanne. On the molecular origin of supercapacitance in nanoporous carbon electrodes. *Nature Materials*, 11:306–310, 2012. doi: 10.1038/nmat3260.

Scientific publications

Author contributions

Paper I: An Exact Ewald Summation Method in Theory and Practice

I participated in developing the theory and wrote the simulation software. I wrote the first draft of the manuscript.

Paper II: Grand canonical simulations of ions between charged conducting surfaces using exact 3D Ewald summations

I participated in developing the theory and writing simulation software. I wrote parts of the manuscript.

Paper III: Overcharging and Free Energy Barriers for Equally Charged Surfaces Immersed in Salt Solutions

I performed some of the calculations and participated in analyzing the results. I write the first draft of the manuscript.

Paper IV: Interactions between conducting surfaces in salt solutions

I performed some of the calculations and participated in analyzing the results. I participated in writing the manuscript.

Paper V: Simulations of phase transitions and capacitance, of simple ionic fluids in porous electrodes.

I performed some of the simulations and participated in analyzing the results.

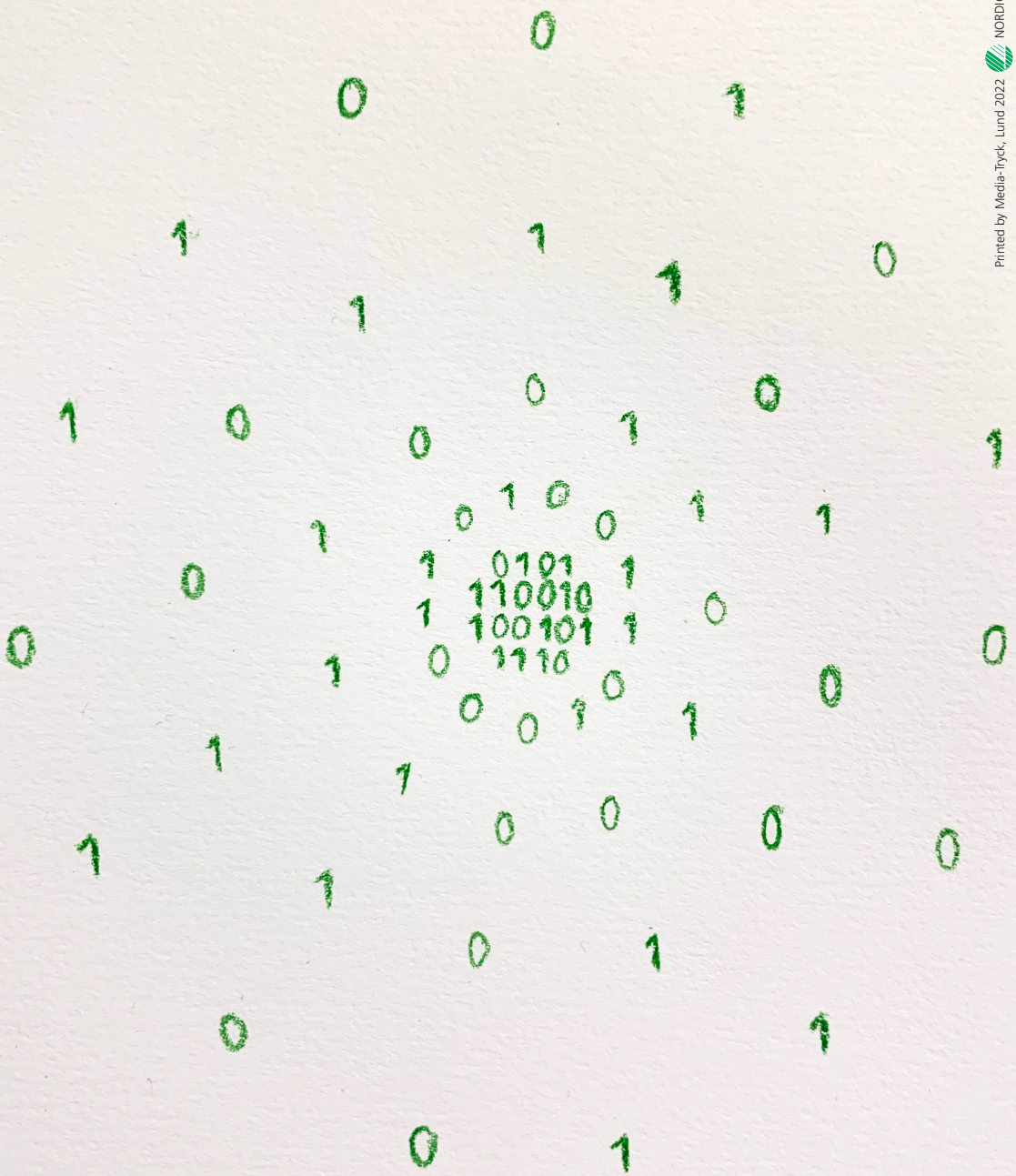

Printed by Media-Tryck, Lund 2022 NORDIC SWAN ECOLABEL 3041 0903

ISBN: 978-91-7422-888-5

Theoretical Chemistry
Department of Chemistry
Faculty of Science
Lund University

LUND UNIVERSITY